User Association and Multi-Connectivity Strategies in Joint Terahertz and Millimeter Wave 6G Systems

Eduard Sopin , Dmitri Moltchanov , Anastasia Daraseliya , Yevgeni Koucheryavy, and Yuliya Gaidamaka

Abstract—**Terahertz (THz) wireless access is considered as a next step towards 6G cellular systems. By utilizing even higher frequency bands than 5G millimeter wave (mmWave) New Radio (NR), they will operate over extreme bandwidth delivering unprecedented rates at the access interface. However, by relying upon pencil-wide beams, these systems will not only inherit mmWave propagation challenges such as blockage phenomenon but introduce their own issues associated with micromobility of user equipment (UE). In this paper, we analyze and compare user association schemes and multi-connectivity strategies for joint 6G THz/mmWave deployments. Differently, from stochastic geometry studies, we develop a unified analytically tractable framework that simultaneously accounts for specifics of THz and mmWave radio part design and traffic service specifics at mmWave and THz base stations (BS). Our results show that (i) for negligible blockers density, $\lambda_B \leq 0.1$ bl./m^2, the operator needs to enlarge the coverage of THz BS by accepting sessions that experience outage in case of blockage (ii) for $\lambda_B > 0.1$ bl./m^2, only those sessions that does not experience outage in case of blockage need to be accepted at THz BS, (iii) THz/mmWave multi-connectivity improves the ongoing session loss probability by $0.1 - 0.4$ depending on the system parameters.**

Index Terms—**5G, 6G, blockage, micromobility, millimeter wave, multi-connectivity, outage, terahertz, user associations.**

I. INTRODUCTION

SIMILARLY to millimeter wave (mmWave) New Radio (NR) systems providing capacity boost for cellular infrastructure in places with high traffic demands [1], terahertz (THz) access systems are expected to be utilized in locations with the need for extraordinary data rates [2]. However, in addition to extreme capacity, these systems bring several unique challenges to system designers, making efficient deployment and utilization of such systems a complex task.

The propagation and link layer specifics of THz communications have been studied fairly well so far. Similarly to mmWave systems, THz communications are subject to blockage phenomenon [3]. In addition to higher free-space propagation losses, THz propagation is also much heavier affected by atmospheric absorption as compared to mmWave band [4]. Finally, by relying upon extremely directional antenna radiation patterns with half-power beamwidth (HPBW) of the main lobe approaching 1°, these systems may suffer from frequent outages due to UE micromobility [5], [6]. These specifics make THz links highly unreliable requiring natural support from other technologies to ensure session service continuity at the THz air interface.

Future THz wireless access systems will target the support of rate-greedy applications such as virtual/augmented reality (VR), 8/16 K streaming, holographic telepresence that are inherently sensitive to outages [7]. To improve session continuity of applications running over inherently unreliable wireless technologies, 3GPP has recently proposed the multi-connectivity functionality [8]. According to it, UE is allowed to maintain two or more active connections to nearby base stations (BS) of the same or different radio access technologies (RAT), referred to as inter- and intra-RAT multi-connectivity, respectively. The intra-RAT multi-connectivity has been studied in detail in context of mmWave 5G NR systems [9]–[12], where it was shown to drastically improve outage performance of UEs. However, the limited coverage of prospective THz BSs as compared to mmWave NR BSs will require very dense deployments to efficiently utilize intra-RAT multi-connectivity.

To improve reliability of user sessions in future 6G THz/mmWave deployments, inter-RAT multi-connectivity operation can be utilized. However, the only other RAT having comparable albeit much smaller resources at the air interface is 5G NR operating in mmWave band. In spite both technologies target similar type of rate-greedy outage-sensitive applications, there is an inherent capacity mismatch between technologies. Thus, one needs to account not only for the radio specifics but for details of the resource allocation process at BSs. Furthermore, differently from the joint usage of microwave (μWave) and mmWave technologies [13], [14], both mmWave and THz RATs are subject to blockage events that require careful design of user association strategies. Finally, THz RAT is also affected by UE micromobility. To the best of the authors' knowledge, there are no studies assessing the use of inter-RAT multi-connectivity in 6G THz/mmWave deployments.

In this paper, we fill the abovementioned gap by evaluating and comparing performance of user association schemes and multi-connectivity strategies in joint THz/mmWave radio access networks. Contrarily to the previous studies of user associations in heterogeneous access systems, we explicitly account for not only radio part specifics of considered technologies including

propagation, dynamic blockage and micromobility effects but the traffic service process at mmWave and THz BSs. The performance of the considered user association schemes and multi-connectivity strategies are assessed and compared based on the user- and system-level metrics including new session loss capabilities, ongoing session loss probability as well as system resource utilization.

The main contributions of our study are:
- a mathematical framework based on stochastic geometry and queuing theory allowing for unified characterization of association schemes and multi-connectivity strategies by accounting for both radio and service part specifics;
- numerical analysis of user association schemes and multi-connectivity strategies for THz/mmWave deployments;
- numerical results showing that: (i) there is trade-off between new and ongoing session loss probabilities that depends on the choice of association and multi-connectivity strategy, (ii) the choice of the optimal association scheme mainly depends on the blockers density, (iii) tolerance of applications to short-term outages caused by antenna misalignment may greatly improve user performance, and (iv) intra-RAT multi-connectivity improves the ongoing session loss probability by approximately $0.1 - 0.4$.

Our paper is organized as follows. In Section III we introduce our system model. Performance evaluation framework is developed in Section IV and parameterized using radio part parameters in Section V. Numerical analysis is conducted in Section VI. Conclusions are drawn in the last section.

II. RELATED WORK

System-level performance analysis of future 6G THz systems has been mainly studied so far by utilizing stochastic geometry approach. The studies mainly concentrated on characterizing impairments produced by blockage and micromobility as well as on the techniques utilized to mitigate them. Specifically, the authors in [15], [16] characterized interference and signal-to-interference plus noise ratio (SINR) at UEs by accounting for blockers density and directional antennas. Further, studies extending those works to deployment specifics have been published, see Shafie et al. [17] for 3D, Wu et al. [18] for indoor deployments, etc. Recently, the authors also investigated the effect of 3GPP multiconnectivity in dynamic blockage environment in [19]. These results have been further extended to account for micromobility in [20]. In both studies, the authors concentrate on capacity and outage probability showing that multiconnectivity improves both metrics.

Much less is known about system-level performance of joint operation of mmWave/THz systems. Among few others, is the study in [21], where the authors formulated the optimization problem of determining user associations in joint mmWave/THz systems to improve UE throughput in these systems. Another similar study targeting associations in these systems is [22], where a coexisting μWave and THz system has been considered. By utilizing system-level simulations heuristic UE associations

algorithms have been proposed. However, similarly to THz-only systems, the abovementioned studies mainly concentrate on elastic traffic patterns.

The main rationale for utilizing mmWave and THz systems jointly is the type of traffic they target. By providing extreme amount of resources at the air interface both RATs target rate-greedy non-elastic applications such as AR/VR, 8/16 K streaming, holographic telepresence [7]. One of the inherent properties of joint mmWave/THz systems is that both of them are subject to dynamic blockage while THz systems may further be affected by micromobility. There are few studies published to date targeting non-elastic traffic in mmWave only systems [12] or mmWave/μWave systems [14] with multiconnectivity support. Among other conclusions, [14] shows that temporal offloading of rate-greedy connections to μWave systems leads to detrimental effects in terms of UE having μWave interface only, while [12] illustrates that mmWave system alone may still lead to non-negligible loss probability of sessions accepted to service.

The conventional analysis tool utilized in the past – stochastic geometry – is no longer sufficient alone for mmWave/THz systems as it inherently assumes elastic traffic. To make conclusions on the performance characteristics of the session service process in joint mmWave/THz systems we need to take into account not only the specifics of the radio part and stochastic factors related to the randomness of channel and UE locations, but the traffic service dynamics at BSs by joining the tools of stochastic geometry and queuing theory.

III. SYSTEM MODEL

In this section, we introduce our system model. We define the deployment, dynamic blockage, propagation, antenna, beamalignment, and micromobility models, and then complement them with the resource allocation and traffic assumptions. Finally, we introduce the user associations and dynamic multi-connectivity assumptions as well as the metrics of interest. The notation used in this paper is provided in Table I.

A. Deployment Model

We assume a mature phase of mmWave NR market penetration by considering a well-provisioned mmWave BS deployment. We tag and consider an arbitrarily chosen circularly-shaped service area of mmWave BS with radius r_M, where r_M is such that no outage happens at the cell boundary in line-of-sight (LoS) blocked state, see Fig. 1. This radius is determined in Section V by utilizing the set of NR modulation and coding schemes (MCS, [23]) and propagation model defined below.

In the coverage area of mmWave BS an operator is assumed to deploy K THz BSs. The geometric locations of these THz BSs are uniformly distributed. The maximal feasible coverage radius of these THz BSs is determined by the propagation model introduced in what follows, while the actual coverage r_T depends on the user associations schemes discussed below. The heights of mmWave and THz BSs are constant and given by $h_{M,B}$ and $h_{T,B}$. The carrier frequencies are denoted by $f_{M,c}$ and $f_{T,c}$, while the available bandwidth – by B_M and B_T. In what follows, we assume that $B_T = \infty$. The rationale behind
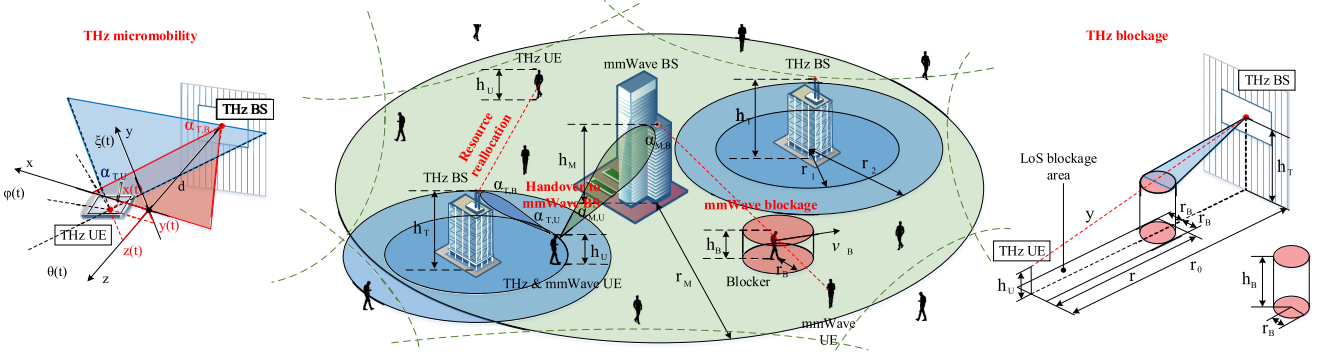
Fig. 1. The considered 6G deployment with joint THz/mmWave BSs.

this assumption is that the bandwidth in cellular systems roughly increases by ten times in each generation and is expected to reach 10+ GHz for 6G THz access. Accounting for limited coverage areas and the rates of forthcoming applications (e.g., 10-40 Gbps for XR/VR, [24]) the capacity of these systems will be sufficient to maintain thousands of simultaneous sessions. Nevertheless, we provide the extension to the case of finite capacity at THz BSs in Appendix A.

B. Blockage, Antenna, and Propagation Models

1) Blockage Modeling: We assume that the LoS between the mmWave/THz BS and the UE can be blocked by humans and buildings. To model the former phenomenon, we adopt a dynamic blockage model. According to it, pedestrians, acting as blockers, move by following a random direction mobility model (RDM, [25]). The speed and run length are v_B m/s and an τ m, respectively. The density of pedestrians is λ_B units/m^2. We model them by cylinders with radius r_B and height h_B. The height of blockers is assumed to be h_B, $h_B \leq h_U$, where h_U is the constant height of UEs. The time-averaged blockage probability is given by [26]

$$p_B(y) = 1 - \exp^{-2\lambda_B r_B \left[\sqrt{y^2 - (h_{\cdot,B} - h_U)^2} \frac{h_B - h_U}{h_{\cdot,B} - h_U} + r_B \right]}, \quad (1)$$

where $h_{\cdot,B}$ is the height of mmWave or THz BS, y is the 3D distance between BS and UE.

In addition to human blockage, we also account for blockage by large stationary objects such as buildings manifesting itself in LoS and nLoS propagation according to 3GPP terminology [27]. We adopt 3GPP Urban Micro (UMi) Canyon-Street model providing the following LoS probability in terms of 2D distance $x = \sqrt{y^2 - (h_{\cdot,B} - h_U)^2}$ between BS and UE

$$p_L(x) = \begin{cases} 1, & x \leq 18\,m, \\ 18x^{-1} + e^{-\frac{x}{36}}(1 - 18x^{-1}), & x > 18\,m. \end{cases} \quad (2)$$

In what follows, we will enumerate the possible blockage states as follows: 0 – (nLoS,blocked), 1 – (LoS,blocked), 2 – (nLoS,non-blocked), 3 – (LoS,non-blocked). The corresponding state probabilities are given by

$$\kappa_0(y) = [1 - p_L(y)]p_B(y), \ \kappa_1(y) = p_L(y)p_B(y),$$

$$\kappa_2(y) = [1 - p_L(y)][1 - p_B(y)], \ \kappa_3(y) = p_L(y)[1 - p_B(y)]. \quad (3)$$

2) Antenna Model: At both BS types we assume planar antenna arrays. By following to [15], [28], we use the cone antenna model, where the width of the beam coincides with the radiation pattern's half-power beamwidth (HPBW). The mean gain over HPBW is known to be [29]

$$G = \frac{1}{\theta_{3db}^+ - \theta_{3db}^-} \int_{\theta_{3db}^-}^{\theta_{3db}^+} \frac{\sin(N_{(\cdot)}\pi\cos(\theta)/2)}{\sin(\pi\cos(\theta)/2)} d\theta, \quad (4)$$

where $N_{(\cdot)}$ is the number of antenna elements.

THz BSs and UEs are equipped with arrays having $N_{T,B,V} \times N_{T,B,H}$ and $N_{T,U,V} \times N_{T,U,H}$ elements, respectively. Similarly, mmWave BS and UEs are equipped with arrays having $N_{M,B,V} \times N_{M,B,H}$ and $N_{M,U,V} \times N_{M,U,H}$ elements, respectively. The array's HPBW, α, is found as $\alpha = 2|\theta_m - \theta_{3db}^{\pm}|$, where $\theta_m = \arccos(-1/\pi)$ is the radiation pattern's maximum, $\theta_{3db}^{\pm} = \arccos[-\pm 2.782/(N_{(\cdot)}\pi)]$ are the $\pm$3-dB points. In practice, one may also use approximation $\alpha = 102/N_{(\cdot)}$ [29].

3) MmWave Propagation Model: To represent the mmWave path loss we differentiate between blockage states defined previously and utilize 3GPP UMi model defined in [27], i.e.,

$$L_{dB}(y) = \begin{cases} 32.4 + \zeta_{M,0}10\log(y) + 20\log f_{M,c}, \text{nLoS,bl.}, \\ 52.4 + \zeta_{M,1}10\log(y) + 20\log f_{M,c}, \text{LoS,bl.}, \\ 32.4 + \zeta_{M,2}10\log(y) + 20\log f_{M,c}, \text{nLoS,nbl.}, \\ 52.4 + \zeta_{M,3}10\log(y) + 20\log f_{M,c}, \text{LoS,nbl.}, \end{cases} \quad (5)$$

where y is the UE-BS distance measured in meters, $f_{M,c}$ is the carrier frequency in GHz, $\zeta_{M,i}$ are path loss exponents. Note that the first value accounts for human blockage attenuation that is reported to vary between 15 and 30 dB [30]. We assume 20 dB of additional losses induced by human blockage.

The model in (5) can be converted to the linear scale, to the form $A_{M,i}y^{-\zeta_{M,i}}$, $i = 0, 1, 2, 3$, where

$$A_{M,0} = A_{M,1} = 10^{2\log_{10}f_{M,c}+5.24}, \ \zeta_{M,0} = \zeta_{M,2} = 3.19,$$

$$A_{M,2} = A_{M,3} = 10^{2\log_{10}f_{M,c}+3.24}, \ \zeta_{M,1} = \zeta_{M,3} = 2.1. \quad (6)$$

TABLE I
NOTATION UTILIZED IN THE PAPER

Notation	Description
$f_{M,c}, f_{T,c}$	mmWave and THz carrier frequencies, GHz
B_M, B_T	mmWave and THz BS bandwidths, Hz
C	requested rate of sessions, Mbps
λ_A	intensity of session arrivals, sess./s/m^2
K	number of THz BSs in the coverage of mmWave BS
λ_B	density of blockers, bl./m^2
r_M, r_T	mmWave/THz BSs coverage radii, m
$h_{M,B}, h_{M,T}$	mmWave/THz BSs heights, m
v_B, h_B, r_B	blocker speed (m/s), height (m), and radius (m)
h_U	UE height, m
P_M, P_T	mmWave/THz BSs emitted power, W
N_0	thermal noise power, dBi
$G_{M,B}$	mmWave BS antenna array gain
$G_{M,U}$	mmWave UE antenna array gain
$A_{M,i}, A_{T,i}$	mmWave/THz path loss coefficients
$C_{M,i}, C_{T,i}$	mmWave/THz propagation constants
$\zeta_{M,1}, \zeta_{M,2}$	mmWave path loss exponents
$p_{M,O}, p_{T,O}$	cell edge outage probability at mmWave/THz BS
$S_{M,\min}, S_{T,\min}$	mmWave/THz SINR outage thresholds, dB
$G_{T,B}$	THz BS antenna array gain
$G_{T,U}$	THz UE antenna array gain
$\zeta_{T,1}, \zeta_{T,2}$	THz path loss exponents
$\Omega_{M,i}, \Omega_{T,i}$	mmWave/THz shadow (log-Normal) fading, dB
$\Upsilon_{M,i}, \Upsilon_{T,i}$	mmWave/THz small-scale (Nakagami-m) fading, dB
I_M, I_T	mmWave/THz interference, dB
r_I	maximum interference radius, m
$M.$	mmWave/THz inter./shadow/small-scale margins, dB
$L_A(f_{T,c}, r)$	absorption loss, dB
$K(f)$	absorption coefficient, m^{-1}
$N_{T,B,V} \times N_{T,B,H}$	THz BS antenna configuration, el.×el.
$N_{T,U,V} \times N_{T,U,H}$	THz UE antenna configuration, el.×el.
$N_{M,B,V} \times N_{M,B,H}$	mmWave BS antenna configuration, el.×el.
$N_{M,U,V} \times N_{M,U,H}$	mmWave UE antenna configuration, el.×el.
$\alpha_{M,B}, \alpha_{M,U}$	mmWave BS/UE antenna array HPBW, °
$\alpha_{T,B}, \alpha_{T,U}$	THz BS/UE antenna array HPBW, °
$\theta_m, \theta_{3db}^{\pm}$	array maximum and ± 3 dB points, °
$p_B(y)$	blockage probability at distance y
$p_L(y)$	LoS probability at distance y
κ_i	State blockage/LoS probabilities at distance y
δ	THz array switching time, s
T_B	THz beamalignment duration, s
T_O	outage tolerance time of applications, s
μ^{-1}	mean service time of sessions, s
$p_{1,r}, p_{2,r}$	session resource requirements pmfs
ν	blockage intensity at mmWave BS, bl./s
ν_M	outage intensity caused by micromobility events/s
ν_B	outage intensity caused by blockage, events/s
$p_{0,1}, p_{0,2}$	outage fraction for on-demand/periodic alignment
$T_{O,1}, T_{O,2}$	outage for on-demand/periodic beamalignment, s
T_A	time to outage due to micrimobility, s
$f_{T_A}(t)$	pdf of time to outage in presence of micromobility
T_U	periodic beamalignment interval, s
β_B	connection recovery intensity for blockage, events/s
β_M	connection recovery intensity for micromob., events/s
ε_j	probability that the UE is assigned the MCS j
p_T	THz UE association probability
$x(t), y(t)$	random displacements processes over x- and y-axis
$\phi(t), \theta(t)$	yaw and pitch rotational mobility processes
J	number of NR MCSs

The value of SINR at the mmWave UE can be written as a weighted function of SINRs in different states as

$$S(y) = \sum_{i=0}^{3} \frac{C_{M,i} y^{-\zeta_{M,i}} \kappa_i(y) \Omega_{M,i} \Upsilon_{M,i}}{N_0 B_M + I_M}, \tag{7}$$

where $C_{M,i} = P_M, G_{M,B} G_{M,U}/A_{M,i}$, P_M is mmWave BS emitted power, $G_{M,B}$ and $G_{M,U}$ are the mmWave BS and UE gains, B_M is the bandwidth of mmWave BS, I_M is the interference, $\Upsilon_{M,i}$ and $\Omega_{M,i}$ are the Nakagami-m small-scale with parameters $V_{M,i}$ and log-Normal shadow fading with standard deviation $\sigma_{M,i}$, y is 3D distance between UE and BS, $\kappa_i(y)$ is the LoS/blockage state probabilities defined in (3).

4) THz Propagation Model: The principal difference between mmWave and THz propagation models is presence of atmospheric absorption [4]. By utilizing the results of [15], the absorption loss is defined as

$$L_A(f, y) = 1/\tau(f_{T,c}, y), \tag{8}$$

where $\tau(f_{T,c}, y)$ is the transmittance of the medium following the Beer-Lambert law, $\tau(f_{T,c}, y) \approx e^{-Ky}$, K is the absorption coefficient that can be computed by utilizing the HITRAN database [31] as shown in [4].

Similarly to (7), SINR at the THz UE can be written as

$$S(y) = \sum_{i=0}^{3} \frac{C_{T,i} e^{-Ky} y^{-\zeta_{T,i}} \kappa_i(y) \Omega_{T,i} \Upsilon_{T,i}}{N_0 B_T + I_T}, \tag{9}$$

where the nature of variables is similar to those defined for mmWave system in (7).

The assumptions regarding propagation, antenna, blockage and interference models can be further extended to fit the needs of a particular deployment. We will concentrate on crucial factors affecting session-level dynamics by causing potential connection interruptions (micromobility and blockage) or drastic long-term change in the required rate (blockage). Specifically, for a given deployment density, one may estimate it by employing stochastic geometry models [32]. Note that the more complex 3GPP multi-path 3D cluster-based model [27] can also be used in the proposed framework as shown in [13]. Finally, more comprehensive blockage models capturing blockage by large stationary objects such as buildings can also be used as discussed in [11].

C. Micromobility and Beamalignment Models

1) Micromobility Model: To represent the micromobility process at UE we utilize the model introduced in [5]. According to it, the micromobility is modeled as a combination of random displacements processes $x(t)$ and $y(t)$ over x- and y-axes, together with the random rotation processes over yaw (normal) and pitch (transverse) axes, $\phi(t)$ and $\theta(t)$. By assuming Brownian motion nature of these processes, the authors in [5] revealed that the probability density function (pdf) of time to outage follows (10), shown at the bottom of the next page, where erfc($\cdot$) is the complementary error function, $\mu_{(\cdot)}$ and $\sigma_{(\cdot)}$ are the parameters of the corresponding displacement and rotation components that can be estimated from the empirical data provided in [6].

2) Beamalignment Model: The ability of applications to tolerate outages caused by micromobility may improve system performance. For this reason, we will explicitly account for the beamalignment time. We consider the hierarchical beamalignment scheme realized via sector scan and in-sector refinement procedures. This approach is utilized in IEEE 802.11ad/ay, where

communications entities perform beamalignment separately by forcing the other side to use the omnidirectional mode. The beamalignment time of this approach is $T_B = (N_{T,B,H} N_{T,B,V} + N_{T,U,H} N_{T,U,V})\delta$, where $N_{T,B,H} N_{T,B,V}$ and $N_{T,U,H} N_{T,U,V}$ are the THz BS and UE antenna array configurations and δ is the array switching time.

D. Associations, Applications, and Multi-Connectivity

1) User Association Schemes: A session associated with UE is assumed to arrive at either mmWave BS or THz BS based on its geometric location and coverage of THz BSs. Particularly, with probability $p_T = K\pi r_T^2 / \pi r_M^2$ session initially arrives to one of the THz BS and with complementary probability $(1 - p_T)$ it arrives to mmWave BS, where K is the number of THz BSs, while coverage radius of THz BS, r_T, depends on the considered association schemes:

- *Outage avoidance, A1.* In this association scheme, only those sessions that do not experience outage in blockage conditions with THz BSs are initially accepted at THz BS. As one may observe, it leads to higher offered traffic load to mmWave BS but may improve service reliability of sessions initially associated with THz BSs, especially, for applications characterized by low micromobility and/or in dense blockage environments.
- *Coverage enhancement, A2.* In this association scheme, one attempts to maximize the number of sessions accepted to THz BSs, admitting even those that may experience outage in blockage conditions. This strategy may enhance the coverage of THz BSs and can be suitable for sparse blockers density conditions.

2) Applications and Multi-Connectivity Strategies: We consider rate-greedy applications specifically tailored for 5 G/6G systems with mmWave and THz resource-rich wireless access, e.g., AR/VR, 8/16 K streaming, holographic telepresence [7]. These applications generate non-elastic traffic, i.e., the requested rate cannot be changed during the session. As described below, we also consider applications that may or may not tolerate outage time $T_O = T_B$ caused by micromobility, where T_B is the beamalignment time at THz BS.

The sessions that initially arrive to mmWave BS are assumed to never change their association point while those, initially accepted at THz BSs, have an option to switch to mmWave BS in case of outage caused by either micromobility or outage or both, depending on the considered multi-connectivity strategy. To make conclusions on the optimal UE behavior in joint

THz/mmWave radio access network we consider the following multi-connectivity strategies:

- *No dynamic multi-connectivity, S1.* For this strategy, we assume that multi-connectivity is not supported at UEs and the initial association point remains unchanged.
- *Blockage avoidance for outage non-sensitive applications, S2.* In this case, we assume that the application may tolerate outages caused by antenna misalignment at THz BS. However, to deal with blockage, UEs support multi-connectivity and the session is rerouted to mmWave BS whenever outage caused by blockage occurs.
- *Blockage avoidance for outage sensitive applications, S3.* This strategy is essentially similar to the previous one except we assume that the application cannot tolerate outage caused by micromobility. Thus, whenever micromobility happens, the session is assumed to be lost.
- *Fully dynamic multi-connectivity, S4.* In fully dynamic multi-connectivity, we assume that outages caused by both blockage and micromobility lead to rerouting of session associated with THz BS to mmWave BS.

In all the considered strategies, where multi-connectivity is supported, the session rerouted to mmWave BS is returned to THz BS, once either the blockage expires or beamalignment is completed. By combining the association schemes and multi-connectivity strategies, one may capture a wide range of potential operational policies in joint THz/mmWave deployments.

E. Traffic, Resources, and Metrics of Interest

1) Traffic and Resources: We assume that the amount of resources available at mmWave BS is R primary resource blocks (PRB) that depends on the bandwidth B_M and the chosen numerology of NR technology [23]. Contrarily, the amount of resources at THz BS is assumed to be sufficient to handle all the arriving sessions, i.e., virtually unlimited due to large bandwidth $B_T >> B_M$ and small coverage $r_T << r_M$.

The session arrival process is Poisson with intensity λ_A sess./m². The overall session arrival intensity is $\lambda_A \pi r_M^2$. An arriving session is associated with UE and each UE is allowed to have at most one active session. The geometric locations of arriving sessions are assumed to be randomly and uniformly distributed within the coverage area of mmWave BS. Each arriving session is assumed to request the bitrate C. The amount of requested resources depends on the location of UE and utilized MCSs and is found in Section V.

$$f_{T_A}(t) = \frac{\frac{e^{-\frac{(\log(t)-\mu_x)^2}{2\sigma_x^2}}}{\sigma_x}\left[2 - \text{erfc}\left(\frac{\mu_y - \log(t)}{\sqrt{2}\sigma_y}\right)\right] + \frac{e^{-\frac{(\log(t)-\mu_y)^2}{2\sigma_y^2}}}{\sigma_y}\left[2 - \text{erfc}\left(\frac{\mu_x - \log(t)}{\sqrt{2}\sigma_x}\right)\right]}{2\sqrt{2\pi}t\left[1 - \frac{1}{2}\text{erfc}\left(\frac{\mu_\phi - \log(t)}{\sqrt{2}\sigma_\phi}\right) + \frac{1}{2}\text{erfc}\left(\frac{\mu_\theta - \log(t)}{\sqrt{2}\sigma_\theta}\right)\right]^{-1}}$$

$$+ \frac{\frac{e^{-\frac{(\log(t)-\mu_\phi)^2}{2\sigma_\phi^2}}}{\sigma_\phi}\left[2 - \text{erfc}\left(\frac{\mu_\theta - \log(t)}{\sqrt{2}\sigma_\theta}\right)\right] + \frac{e^{-\frac{(\log(t)-\mu_\theta)^2}{2\sigma_\theta^2}}}{\sigma_\theta}\left[2 - \text{erfc}\left(\frac{\mu_\phi - \log(t)}{\sqrt{2}\sigma_\phi}\right)\right]}{2\sqrt{2\pi}t\left[1 - \frac{1}{2}\text{erfc}\left(\frac{\mu_x - \log(t)}{\sqrt{2}\sigma_x}\right) + \frac{1}{2}\text{erfc}\left(\frac{\mu_y - \log(t)}{\sqrt{2}\sigma_y}\right)\right]^{-1}} \tag{10}$$

A session initially arriving to mmWave can be lost due to insufficient amount of resources available. Note that during the service process, a session initially accepted to mmWave BS is also subject to blockage. However, the coverage of mmWave BS is chosen such that these blockage events do not lead to outage. Nevertheless, sessions initially associated with mmWave BS may also be lost during the service as blockage events lead to resource reallocation due to the use of different MCSs. According to our assumptions, a session initially arriving to THz BS is never lost upon arrival. However, depending on the association scheme and multi-connectivity strategy it might be lost as a result of rerouting to mmWave BS or when no actions taken in case of outage.

2) Metrics of Interest: For the considered system, we are interested in identifying the optimal association scheme and multi-connectivity strategy for different environmental conditions and applications. We will base our conclusions on the following key performance indicators: (i) new session loss probability, i.e., the probability that a newly arriving session is lost at mmWave BS due to the lack of resources, (ii) ongoing session loss probability, i.e., the probability that a session is lost during the service as a result of the lack of resources at mmWave BS while being rerouted or as a result of outage and/or micromobility at THz BS, and, finally, (iii) mmWave BS resource utilization.

IV. PERFORMANCE EVALUATION FRAMEWORK

In this section, we formulate our framework. We start with formalization of the general problem. Then, we consider the simplest case when no dynamic multi-connectivity is performed. Further, we address the general case when multi-connectivity is performed in case of outage caused by both micromobility and blockage. Results for other multi-connectivity strategies are finally provided.

A. Model Formalization

Consider a queuing network with $K + 1$ nodes, where nodes $1, 2, \ldots, K$ represent THz BSs, while the node $K + 1$ models mmWave BS. Node k receives a Poisson arrival flow of sessions with intensity λ_k, $k = 1, 2, \ldots, K + 1$. Service times of the sessions are exponentially distributed with parameter μ. Note that the arrival intensities are obtained as follows

$$\lambda_{K+1} = (1 - p_T)\lambda_A \pi r_M^2, \; \lambda_k = \frac{p_T \lambda_A \pi r_M^2}{K}, \; k = 1, 2, \ldots, K, \tag{11}$$

where $p_T = K\pi r_T^2 / \pi r_M^2$ is the THz association probability.

Since the amount of resources at THz BSs is assumed to be sufficient to handle arrival traffic load, nodes $1, 2, \ldots, K$ are modeled as the infinite server queuing systems, and node $K + 1$ – by the loss queuing system with random resource requirements (ReLS, [33]) with N servers and R PRBs. Here, servers represent the maximum number of simultaneously supported sessions at a single mmWave BS. Sessions that arrive initially to the node $K + 1$ are not redirected to any other node. Each arriving session requires not only a server, but also a random amount of resources according the pmfs $\{p_{1,r}\}$ and

$\{p_{2,r}\}$, $r \geq 0$ in case of initial arrival and redirection from other nodes, respectively. If the amount of currently available resources is not sufficient to meet the resource requirements upon arrival or redirection of a session, the session is dropped.

Each session that is served on node $K + 1$ is associated with a Poisson flow of events with intensity ν caused by the blockage state changes. Arrival of an event triggers resource reallocation of the session, i.e., the session releases previously occupied resources, generates new amount of required resources and tries to occupy them again. If there are no sufficient free resources at node $K + 1$, the session is dropped.

Each session at nodes $1, 2, \ldots, K$ is associated with two Poisson flows of events with intensities ν_B and ν_M that represent the intensity of outages caused by blockage and micromobility, respectively. In what follows, we will refer to them as b-type and m-type of events. The duration of the outage caused by blockage and micromobility events is approximated by exponential distributions with parameters β_B and β_M, respectively. Depending on the system response to blockage and micromobility events, we consider four multi-connectivity strategies introduced in Section III. Below, we consider user association scheme A2, where the coverage of THz BS is such that users may experience outage in case of blockage. Association scheme A1 is analyzed similarly by recalculating the THz BS association probability p_T and setting the intensity of b-type of events ν_B to zero. Note that the proposed framework can be modified to capture the case of "sub-6 GHz+mmWave" system operation. To produce this scenario, one needs to disable blockage at mmWave system to emulate a microwave BS but still account for blockage at THz BSs that now become mmWave BSs.

B. Fully Dynamic Multi-Connectivity Strategy, S4

1) Parametrization: In this strategy, sessions that originally arrive to nodes $k = 1, 2, \ldots, K$ (THz BSs) switch to node $K + 1$ upon arrival of b- or m-type of events and return back immediately when the blockage or beamalignment is over given that the service time is still not completed. Therefore, there are two arrival flows at node k representing the initial arrivals (primary sessions) and the arrivals returning from node $K + 1$ (secondary sessions). According to the memoryless property of the exponential distribution, the residual service times of secondary sessions have the same distribution as the primary sessions. The arrival intensities of the primary and secondary sessions at node k are λ_k and $\gamma_k = \gamma_{B,k} + \gamma_{M,k}$, respectively, where λ_k is provided in (11), while $\gamma_k, \gamma_{B,k}, \gamma_{M,k}$ will be defined below. The overall intensity of sessions leaving the system is $\mu + \nu_B + \nu_M$. The mean number of sessions $\bar{N}_k$ at node k is thus

$$\bar{N}_k = \frac{\lambda_k + \gamma_k}{\mu + \nu_B + \nu_M}. \tag{12}$$

The service process at node $K + 1$ (mmWave BS) is described by a loss system with random resource requirements [33], [34]. The original service model and the proposed queuing formalization are illustrated in Fig. 2. In the considered multi-connectivity strategy, node $K + 1$ serves the sessions that originally arrive to it, as well as the sessions that are rerouted from nodes
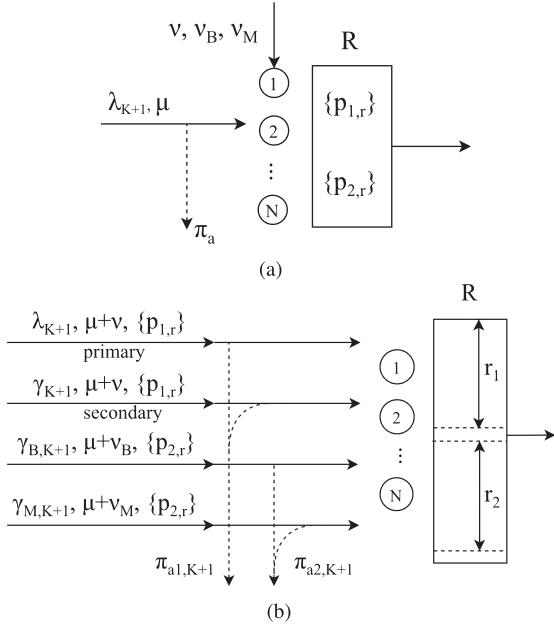
Fig. 2. Original and equivalent ReLS models for node $K + 1$. (a) Original system with events. (b) Equivalent system with additional arrival flows.

$k = 1, 2, \ldots, K$ during outage periods. Only those sessions that originally arrive to the node $K + 1$ suffer from blockage at this node and, thus, similarly to the previously considered strategy, the resource reallocation upon arrival of b-type of events is modeled by additional arrival flow of secondary session. Overall, we define the following arrival flows: (i) initial arrivals (primary sessions) with intensity λ_{K+1}, (ii) arrivals of secondary sessions with intensity $\gamma_{K+1} = \bar{N}_{K+1}\nu$, and (iii) arrivals of rerouted sessions from nodes $k = 1, 2, \ldots, K$ as a result of outage caused by either blockage with intensity $\gamma_{B,K+1}$ or micromobility with intensity $\gamma_{M,K+1}$. The secondary session arrival intensity equals to the total intensity of b-type event arrivals, that is,

$$\gamma_{K+1} = \bar{N}_{1,K+1}\nu. \tag{13}$$

The intensities $\gamma_{B,K+1}$ and $\gamma_{M,K+1}$ are obtained as the sum of all rerouting intensities from nodes $k = 1, 2, \ldots, K$, i.e.,

$$\gamma_{B,K+1} = \sum_{k=1}^{K} \bar{N}_k\nu_B, \quad \gamma_{M,K+1} = \sum_{k=1}^{K} \bar{N}_k\nu_M. \tag{14}$$

The service intensity of primary and secondary sessions is $\mu + \nu$, while the service intensities of the rerouted sessions are $\mu + \nu_B$ and $\mu + \nu_M$. The resource requirements of the primary and secondary sessions obey the pmf $\{p_{1,r}\}$, $r \geq 0$, while those of rerouted sessions follow the pmf $\{p_{2,r}\}$, $r \geq 0$. Since the resource requirements of primary and secondary sessions are equal, they can be aggregated in a single arrival flow with the offered traffic load

$$\rho_1 = \frac{\lambda_{K+1} + \gamma_{K+1}}{\mu + \nu}. \tag{15}$$

The rerouted sessions are characterized by the same resource requirements distribution, so they may also be aggregated in one

flow with the offered load

$$\rho_2 = \frac{\gamma_{B,K+1}}{\mu + \beta_B} + \frac{\gamma_{M,K+1}}{\mu + \beta_M}. \tag{16}$$

2) Solution and Metrics: The following theorem holds.

Theorem 1: The stationary probabilities $q_{n_1,n_2}(r_1, r_2)$ that there are n_1 primary or secondary sessions occupying r_1 resources and n_2 rerouted sessions that totally occupy r_2 resources have the following form [34]

$$q_{n_1,n_2}(r_1, r_2) = q_0 \frac{\rho_1^{n_1}}{n_1!} \frac{\rho_2^{n_2}}{n_2!} p_{1,r_1}^{(n_1)} p_{2,r_2}^{(n_2)},$$

$$0 \leq n_1 + n_2 \leq N, 0 \leq r_1 + r_2 \leq R, \tag{17}$$

where the probability q_0 is computed as

$$q_0 = \left(\sum_{0 \leq n_1 + n_2 \leq N} \frac{\rho_1^{n_1}}{n_1!} \frac{\rho_2^{n_2}}{n_2!} \sum_{0 \leq r_1 + r_2 \leq R} p_{1,r_1}^{(n_1)} p_{2,r_2}^{(n_2)} \right)^{-1}. \tag{18}$$

Proof: The proof is provided in [34]. ∎

Having obtained the stationary distribution, we can evaluate the considered performance metrics. Particularly, the mean number of sessions of each aggregated flow is given by

$$\bar{N}_{i,K+1} = \sum_{0 \leq n_1 + n_2 \leq N} \sum_{0 \leq r_1 + r_2 \leq R} n_i q_{n_1,n_2}(r_1, r_2), \quad i = 1, 2. \tag{19}$$

The loss probabilities of sessions initially associated with $K + 1$ node (mmWave BS) and of rerouted sessions from node k (THz BSs) are then provided by

$$\pi_{a1,K+1} = 1 - \sum_{0 \leq n_1 + n_2 \leq N-1} \sum_{0 \leq r_1 + r_2 \leq R} q_{n_1,n_2}(r_1, r_2) \sum_{j=0}^{R-r_1-r_2} p_{1,j},$$

$$\pi_{a2,K+1} = 1 - \sum_{0 \leq n_1 + n_2 \leq N-1} \sum_{0 \leq r_1 + r_2 \leq R} q_{n_1,n_2}(r_1, r_2) \sum_{j=0}^{R-r_1-r_2} p_{2,j}. \tag{20}$$

Denote by $\bar{N}_{2B,K+1}$ the mean number of sessions that are rerouted to node $K + 1$ due to blockage, and by $\bar{N}_{2M,K+1}$ – the mean number of sessions that are rerouted to node $K + 1$ due to micromobility. Then, the arrival intensity of secondary sessions at node k (i.e., the intensity of sessions returning back to their original node k) is given by

$$\gamma_k = \frac{\bar{N}_k\nu_B}{\gamma_{B,K+1}} \bar{N}_{2B,K+1}\beta_B + \frac{\bar{N}_k\nu_M}{\gamma_{M,K+1}} \bar{N}_{2M,K+1}\beta_M, \tag{21}$$

where $\bar{N}_k\nu_B/\gamma_{B,K+1}$ and $\bar{N}_k\nu_M/\gamma_{M,K+1}$ are the fractions of sessions that are rerouted from node k to node $K + 1$, while $\bar{N}_{2B,K+1}\beta_B$ and $\bar{N}_{2M,K+1}\beta_M$ are the total intensities of sessions returning back to their original node from node $K + 1$. The mean number of sessions can be estimated by equating session acceptance and session departure rates, i.e.,

$$\gamma_{B,K+1}(1 - \pi_{a2,K+1}) = \bar{N}_{2B,K+1}(\mu + \beta_B), \tag{22}$$

$$\gamma_{M,K+1}(1 - \pi_{a2,K+1}) = \bar{N}_{2M,K+1}(\mu + \beta_M), \tag{23}$$

which leads to

$$\gamma_k = \frac{\bar{N}_k \nu_B (1 - \pi_{a2,K+1})\beta_B}{\mu + \beta_B} + \frac{\bar{N}_k \nu_M (1 - \pi_{a2,K+1})\beta_M}{\mu + \beta_M}. \tag{24}$$

The probability that a session initially arriving at node $K + 1$, is lost upon arrival is given by the loss probability of the primary sessions, i.e.,

$$\pi_N = \pi_{a1,K+1}. \tag{25}$$

The probability that a session initially arriving at node $K + 1$, is lost during the service is evaluated similarly to (34), that is,

$$\pi_{s,K+1} = \lim_{t \to \infty} \frac{\bar{N}_{1,K+1}\nu\pi_N t}{\lambda_{K+1}(1 - \pi_N)t} = \frac{\bar{N}_{1,K+1}\nu\pi_N}{\lambda_{K+1}(1 - \pi_N)}. \tag{26}$$

The mean number of occupied resources at node $K + 1$ is

$$\bar{R} = \sum_{1 \le n_1 + n_2 \le N} (n_1 + n_2) \sum_{0 \le r_1 + r_2 \le R} q_{n_1, n_2}(r_1, r_2). \tag{27}$$

The sessions that originally arrive at nodes $k = 1, 2, \ldots, K$ can be lost only during rerouting to node $K + 1$. So, their loss probability $\pi_{s,k}$ is equal to the ratio of lost sessions to the accepted sessions as time $t \to \infty$, i.e.,

$$\pi_{s,k} = \lim_{t \to \infty} \frac{\bar{N}_k(\nu_B + \nu_M)\pi_{a2,K+1}t}{\lambda_k t} = \frac{\bar{N}_k(\nu_B + \nu_M)\pi_{a2,K+1}}{\lambda_k}. \tag{28}$$

Finally, by averaging over all the nodes, the total ongoing session loss probability π_O is obtained according to (35). The procedure described above is iterative in nature, see Appendix B for details.

C. No Dynamic Multi-Connectivity Strategy, S1

1) Parameterization: This strategy is a degenerate case of S3, as the service processes at all nodes are independent of each other. Then, the probabilities b_k and m_k of session loss upon arrival of a b- or m-type of events at nodes $k = 1, 2, \ldots, K$ are equal to the probability that the outage time exceeds the outage tolerance time, T_O,

$$b_k = e^{-\beta_B T_O}, \ m_k = e^{-\beta_M T_O}, \ k = 1, 2, \ldots, K. \tag{29}$$

The total intensity of sessions leaving the nodes $k = 1, 2, \ldots, K$ is $\mu + \nu_B b_k + \nu_M m_k$, where μ is the intensity of service completions, $\nu_B b_k$ and $\nu_M m_k$ are the service interruption intensities caused by blockage and micromobility, respectively. The probability $\pi_{s,k}$ of session loss during the service is

$$\pi_{s,k} = \frac{\nu_B b_k + \nu_M m_k}{\mu + \nu_B b_k + \nu_M m_k}, \quad k = 1, 2, \ldots, K. \tag{30}$$

The service process at node $K + 1$ can be described by a loss system with random resource requirements [34], where sessions occupy a server and a random amount of resources. Recall, that sessions at the node $K + 1$ are associated with b-type of events only. Upon arrival of an event, a session releases the occupied resources, generates new resource requirements according to the same pmf $\{p_{1,r}\}$, $r \ge 0$ and tries to re-enter the system. If the

node $K + 1$ has sufficient amount of unoccupied resources to meet the new resource requirements, it is accepted for further service. Otherwise, it is lost during the service.

2) Solution and Metrics: The following theorem holds true.

Theorem 2: The mean number of sessions at the node $K + 1$ (mmWave BS) obeys

$$\bar{N}_{K+1} = q_0 \sum_{n=0}^{N} n \frac{(\lambda_{K+1} + \bar{N}_{K+1}\nu)^n}{(\mu + \nu)^n n!} \sum_{r=0}^{R} p_{1,r}^{(n)}, \tag{31}$$

where the probability q_0 is provided by

$$q_0 = \left(1 + \sum_{n=1}^{N} \frac{(\lambda_{K+1} + \bar{N}_{K+1}\nu)^n}{(\mu + \nu)^n n!} \sum_{r=0}^{R} p_{1,r}^{(n)} \right)^{-1}, \tag{32}$$

$p_{1,r}^{(n)}$ is the probability that n sessions occupy r resources that can be obtained from the pmf $\{p_{1,r}\}$, $r \ge 0$ using convolution.

Proof: The proof is provided in [34]. ∎

We are now in position to proceed with the metrics of interest. Since the resource requirements of secondary sessions are characterized by the same pmf as the primary ones, the new session loss probability π_N is given by

$$\pi_N = 1 - q_0 \sum_{n=0}^{N-1} \frac{(\lambda_{K+1} + \bar{N}_{K+1}\nu)^n}{(\mu + \nu)^n n!} \sum_{r=0}^{R} p_{1,r}^{(n+1)}, \tag{33}$$

while the ongoing session loss probability at node $K + 1$ is

$$\pi_{s,K+1} = \lim_{t \to \infty} \frac{\bar{N}_{K+1}\nu\pi_N t}{\lambda_{K+1}(1 - \pi_N)t} = \frac{\bar{N}_{K+1}\nu\pi_N}{\lambda_{K+1}(1 - \pi_N)}, \tag{34}$$

where $\bar{N}_{K+1}\nu\pi_N t$ is the number of the secondary sessions lost during time t and $\lambda(1 - \pi_N)t$ is the number of accepted sessions during time t. By averaging over mmWave and THz sessions, one obtains the ongoing session loss probability as

$$\pi_O = \frac{\lambda_{K+1}(1 - \pi_N)}{\lambda_{K+1}(1 - \pi_N) + \sum_{k=1}^{K} \lambda_k} \pi_O(mmW) +$$
$$+ \frac{\sum_{k=1}^{K} \lambda_k}{\lambda_{K+1}(1 - \pi_N) + \sum_{k=1}^{K} \lambda_k} \pi_O(THz), \tag{35}$$

where $\pi_O(mmW)$ is the ongoing mmWave session loss probability, which is given by (34), and $\pi_O(THz)$ is the ongoing THz session loss probability, which is derived by averaging over all K THz nodes, i.e.,

$$\pi_O(THz) = \frac{\sum_{k=1}^{K} \lambda_k \pi_{s,k}}{\sum_{k=1}^{K} \lambda_k}. \tag{36}$$

Finally, the mean number of occupied resources $\bar{R}$ at the node $K + 1$ (mmWave BS) is

$$\bar{R} = q_0 \sum_{n=0}^{N} \frac{(\lambda_{K+1} + \bar{N}_{K+1}\nu)^n}{(\mu + \nu)^n n!} \sum_{r=0}^{R} r p_{1,r}^{(n)}. \tag{37}$$

Note that the sums in (31), (33), and (37) are evaluated using the convolution algorithm [35]. The user association scheme A1 is analyzed by setting $\nu_B = 0$ and recalculating r_T.

D. Blockage Avoidance Strategies, S2/S3

In the blockage avoidance strategies, the system behavior is similar to the fully dynamic multi-connectivity strategy. The difference is that the sessions at the nodes $k = 1, 2, \ldots, K$ are not rerouted to the $K + 1$ node upon m-type event arrivals implying that $\gamma_{M,K+1} = 0$. Besides, the arrival intensity γ_k of secondary sessions at node k in (24) takes the form

$$\gamma_k = (\bar{N}_k \nu_B (1 - \pi_{a2,K+1}) \beta_B)/(\mu + \beta_B), \qquad (38)$$

where the mean number of sessions at the nodes $k = 1, 2, \ldots, K$ is evaluated as follows

$$\bar{N}_k = (\lambda_k + \gamma_k)/(\mu + \nu_B + \nu_M m_k), \qquad (39)$$

where m_k is the probability that the beamalignment time exceeds the outage tolerance time T_O. Note that for outage non-sensitive sessions (strategy S2) we have $m_k = 0$, while $m_k = 1$ otherwise (strategy S3).

For the metrics of interest, the only difference from Section IV-B is the loss probability $\pi_{s,k}$ during the service of those sessions that initially arrive to the nodes $k = 1, 2, \ldots, K$. For the considered strategy, it takes the following form

$$\pi_{s,k} = \bar{N}_k (\nu_B \pi_{a2,K+1} + \nu_M m_k)/\lambda_k. \qquad (40)$$

All other expressions and metrics remain unchanged.

V. Framework Parameterization

In this section, the developed performance evaluation framework is parameterized. The required parameters include: (i) the coverage radii of mmWave and THz, r_M and r_T, (ii) the pmfs of the amount of requested resources by a session at mmWave BS, $\{p_{1,r}\}$ and $\{p_{2,r}\}$, $r \geq 0$, (iii) the intensity of UE state changes between LoS blocked and non-blocked states at mmWave and THz BS, ν and ν_B, and (iv) the intensity of state changes at THz BS caused by micromobility ν_M.

We specifically note that propagation, blockage and antenna models with different complexity can be utilized to derive the abovementioned parameters. Depending on the models' complexity one may need to utilize simulation studies or derive those parameters analytically. In what follows, we sketch the procedure for the models introduced in Section III and also provide approximations for simplified ones.

A. Interference Calculation

To proceed with characterizing mmWave and THz service areas and resources requested by sessions at BSs, we first need to characterize interference component in (7). Recalling that we consider future dense deployments of mmWave BSs organizing a cellular structure with 6 neighboring cells utilizing the same frequency, the intercell interference at a randomly chosen UE in the cell coverage can be approximated by

$$I_M = \sum_{i=1}^{6} \sum_{j=0}^{3} C_{M,i} y_i^{-\zeta_{M,i}} k_i(y_i) \Omega_{M,i} \Upsilon_{M,i}, \qquad (41)$$

where y_i are the distances to interfering BSs in adjacent cells.

Note that (41) involves three random variables, small-scale fading $\Upsilon_{M,i}$ having normalized Gamma distribution [36] describing Nakagami-m fading, shadow fading $\Omega_{M,i}$ having log-Normal distribution, and random distances y_i. Observe, the distribution in (41) can be principle be obtained using random variable (RV) transformation technique [37]. However, in the considered deployment y_i are correlated as they have the same random point associated with the arbitrarily chosen UE making this procedure infeasible requiring simulation study.

One feasible approximation would be to utilize interference margin M_I estimated assuming Poisson point process deployment of mmWave BS. By following [15] the moments of interference are provided by the celebrated Campbell theorem

$$E[I_M^n] = \int_{r_B}^{r_I} \sum_{j=0}^{3} C_{M,i} y^{-\zeta_{M,i}} p_C k_i(y) 2\lambda \pi y \, dy, \qquad (42)$$

where r_B is the radius of the blocker, $p_C = \alpha_{M,B} \alpha_{M,U}/4\pi^2$ is the exposure probability, $\alpha_{M,B}$ and $\alpha_{M,U}$ are the mmWave BS and UE HPBWs, r_I is radius such that the interference from BS located farther away than r_I is less than the noise power.

When considering THz BS having finite capacity, the interference for THz UE can be estimated similarly. Furthermore, we emphasize that the approximations in (41) and (42), based on the stochastic geometry, does not account for the fact that mmWave BS resources are not always fully utilized.

B. Effective Coverage Radii

1) MmWave BS Coverage: The coverage of mmWave BSs, r_M, is determined by the deployment density in a given environment and is upper bounded by the maximal feasible coverage radius. Since THz systems are expected to be deployed at the mature phase of 5G mmWave NR deployments, we assume a cellular deployment of mmWave BSs. In these conditions r_M can be determined such that no more than $p_{M,O} << 1$, fraction of cell edge UEs are in outage conditions.

Consider the SINR outage threshold $S_{M,\min}$ representing the minimum SINR value for NR MCS schemes [23]. We determine the cell radius r_M based on the worst possible case, when UE is in (nLoS,blocked) state. Using the propagation model in (7) for this state, we can write

$$S_{M,\min} = \frac{C_{M,0} \Omega_{M,0} \Upsilon_{M,0}}{N_0 B_M + I_M} (r_M^2 + [h_{M,B} - h_U]^2)^{-\zeta_{M,0}}, \qquad (43)$$

and then solve with respect to r_M obtaining

$$r_M = \sqrt{\left(\frac{C_{M,0} \Omega_{M,0} \Upsilon_{M,0}}{(N_0 B_M + I_M) S_{M,\min}}\right)^{2/\zeta_{M,0}} - (h_{M,B} - h_U)^2}. \qquad (44)$$

The problem of determining r_M reduces to finding distribution of the function of three RVs, I_M, $\Omega_{M,0}$ and $\Upsilon_{M,0}$. Similarly to the interference analysis, this is infeasible analytically and one needs to resort to simulation. However, by introducing interference, M_{I_M}, calculated as the first moment in (42), shadow fading margin, $M_{\Omega_{M,0}}$, taken from [27], and small-scale fading
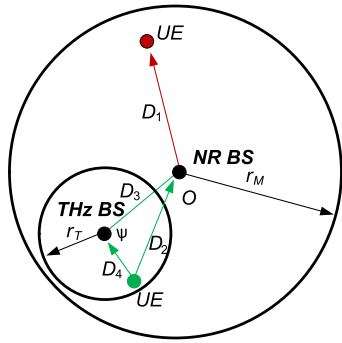
Fig. 3.   Distances in the considered deployment.

margin, $M_{\Upsilon_{M,0}}$, one may use the following approximation,

$$r_M$$

$$= \sqrt{ \left[\frac{C_{M,0}S_{M,\min}^{-1}}{N_0 B_M + M_{I_M} + M_{\Omega_{M,0}} + M_{\Upsilon_{M,0}}} \right]^{2/\zeta_{M,0}} - (h_{M,B} - h_U)^2 }.$$

2) THz BS Coverage: For a given r_M, the coverage radius of THz BS, r_T, heavily affects THz BS association probability, $p_T = K\pi r_T^2/\pi r_M^2$. Having higher r_T leads to better offloading gains to bandwidth-rich THz BSs but may also result in higher frequency of session rerouting to mmWave BS. For user association scheme A1, where only those sessions that do not experience outage in blockage conditions are initially accepted to THz BSs, the coverage radius r_T is computed similarly to mmWave BS above. For coverage enhancement association scheme A2, one needs to replace the propagation model with the model corresponding to nLoS non-blocked conditions in the calculations of the THz BS coverage radius r_T.

C. Resource Request Characterization

1) Sessions Initially Arriving to Mmwave BS: For the general propagation model defined in (7), we recommend using the simulation studies to obtain SINR distribution. However, utilizing the interference, shadow and small-scale fading margins, one may proceed with the approximate analysis below.

Consider sessions that are initially associated with mmWave BS, see Fig. 3. Recall that geometric locations of these sessions are uniformly distributed in the coverage area of mmWave BS. Hence, two-dimensional distance to the mmWave BS can be approximated by $f_{D_1}(x) = 2x/r_M^2$, $0 < x < r_M$. Therefore, the pdf of the 3D distance, Y_1, is

$$f_{Y_1}(y) = 2y/r_M^2, \; y \in (|h_{M,B} - h_U|, Q), \qquad (45)$$

where $Q = \sqrt{r_M^2 + (h_{M,B} - h_U)^2}$ leading to the CDF $F_{Y_1}(y)$

$$F_{Y_1}(y) = \frac{y^2 - (h_{M,B} - h_U)^2}{r_M^2}, \; y \in [|h_{M,B} - h_U|, Q]. \quad (46)$$

Observe that SINR is a decreasing function of y. Thus, SINR CDF in state i can be written by utilizing the distance Y_1,

$$F_{S_i}(s) = Pr\left\{C_{M,i}y^{-\zeta_{M,i}} < s\right\} = 1 - F_{Y_1}\left(\sqrt[\zeta_{M,i}]{C_{M,i}/s}\right),$$
$$(47)$$

where $C_{M,i} = C_{M,i}/(N_0 B_M + M_{I_M} + M_{\Omega_{M,i}} + M_{\Upsilon_{M,i}})$.

Now, the SINR CDF in state i is given by

$$F_{S_i}(s) = \frac{Q^2 - \left(\frac{C_{M,i}}{s}\right)^{\frac{2}{\zeta_{M,i}}}}{r_M^2}, \; \frac{C_{M,i}}{Q^{\zeta_{M,i}}} \le s < \frac{C_{M,i}}{(h_{M,B} - h_U)^{\zeta_{M,i}}}.$$
$$(48)$$

The final SINR CDF is obtained by weighting individual branches with the blockage probability as in (7). Finally, we define $S_j, j = 1, 2, \ldots, J$, to be SINR boundaries for MCS mapping [23] and also let ϵ_j be the probability that the session is associated with MCS j and requires r_j PRBs. By utilizing the SINR CDF $F_S(s)$, we have

$$\epsilon_j = F_S(S_{j+1}) - F_S(S_j), \; j = 1, 2, \ldots, J, \qquad (49)$$

and the probability ϵ_j that a session requests r_j PRBs can now be used to obtain the resource requirements pmf $\{p_{1,r}\} \; r \ge 0$.

2) Sessions Initially Arriving to THz BS: Consider now UE that is initially associated with THz UE and determine its resource requirements at mmWave BS. The only principal difference compared to the abovementioned analysis is that the pdf of 2D distance from UE to mmWave BS, $f_{D_2}(x)$, is different from $f_{D_1}(x)$. It can be found by applying the cosine theorem to the triangle organized by sides D_2, D_3, and D_4, as illustrated in Fig. 3, that is,

$$D_2 = \sqrt{D_3^2 + D_4^2 - 2D_3 D_4 \cos \psi}, \qquad (50)$$

where pdf of components are given by

$$f_{D_3} = 2x/r_M^2, \; f_{D_4} = 2x/r_T^2, \; f_\psi(x) = 1/2\pi. \qquad (51)$$

The pdf $f_{D_2}(x)$, corresponding to (50) can be obtained by using the non-linear transformation of RVs, see, e.g., [37]. Once $f_{D_2}(x)$ is obtained the resource request pmf at mmWave BS of UEs that are initially associated with THz BSs $\{p_{2,r}\} \; r \ge 0$, can be determined similarly to that of UEs initially associated with mmWave BS.

D. Intensities of UE State Changes

Recall, that sessions that are initially associated with THz BSs are allowed to utilize multi-connectivity functionality by switching to mmWave BS in case of outages. The latter may occur as a result of two phenomena: (i) blockage and (ii) micromobility. Let ν_B and ν_M be the corresponding intensities of these events. Note that those sessions that are initially associated with mmWave BS are also subject to blockage events with intensity ν.

1) Blockage Intensity At THz/mmWave BSs: We first need to convert the spatial density of blockers, λ_B, into temporal intensity of blockers entering the blockage zone α. By utilizing

the results in [26] we first determine the mean perimeter of the LoS blockage zone as follows

$$P_L(x) = 4r_B + 2x(h_B - h_U)(h_{T,B} - h_U), \quad (52)$$

where x is 2D distance between BS and UE.

Now, consider the unit area around the LoS blockage zone. A blocker located in this zone and moving according to the RDM model with speed $v_B = 1$ m/s enters the LoS blockage area in approximately 2/5 of cases in a unit time. Thus, the temporal intensity of blockers entering the LoS blockage zone associated with UE located at 2D distance x from THz BS is

$$\alpha(x) = 2\lambda_B v_B [4r_B + 2x(h_B - h_U)(h_{T,B} - h_U)]/5. \quad (53)$$

Let further $\Psi_B(x)$ and $\Phi_B(x)$ be the random blocked and non-blocked periods. It has been shown in [38] that $\Phi_B(x)$ following exponential distribution with parameter $\alpha(x)$, i.e., $E[\Phi_B(x)] = 1/\alpha(x)$. The non-blocked period duration coincides with the busy period in M/G/∞ queuing system with arrival intensity $\alpha(x)$ and service times corresponding to the time a single blocker spends in the LoS blockage zone [38]. Recalling that the length of the LoS blockage zone is much greater than its width, the latter can be approximated by $2r_B/v_B$. By further utilizing M/M/∞ approximation for M/G/∞ we can write down closed-form approximation for the mean LoS blocked period in the following form [39]

$$E[\Psi(x)] = (e^{-\alpha(x)v_B/2r_B} - 1)/\alpha(x). \quad (54)$$

In the outage avoidance association scheme A1 no UEs experience outage conditions as a result of blockage at THz BS. For, coverage enhancement scheme A2, the intensity of UE state changes leading to outage can be found as

$$\nu_B = \int_{r_{T,1}}^{r_{T,2}} (\alpha^{-1}(x) + [\alpha^{-1}(x)e^{-\alpha(x)v_B/2r_B} - 1])^{-1}dx, \quad (55)$$

where $r_{T,1}$ and $r_{T,2}$ are THz BS coverage radii corresponding to A1 and A2 association schemes. Note that intensity of the blockage process at mmWave BSs can be found similarly except for the lower integration limit that has to be set of the minimum separation distance between mmWave BS and UE.

2) Micromobility Intensity: The intensity of UE outages at THz BS caused by micromobility can be found by utilizing the results of [5]. For on-demand and periodic beamalignment schemes, the reported fractions of time in outage are

$$p_{O,1} = \int_0^\infty \frac{T_B}{t + T_B} f_{T_A}(t)dt,$$

$$p_{O,2} = \frac{T_B[1 - F_{T_A}(T_U)]}{T_U + T_B} + \int_0^{T_U} \frac{T_U + T_B - t}{T_U + T_B} f_{T_A}(t)dt, \quad (56)$$

correspondingly, where T_B is the beamalignment time, T_U is the regular beamalignment interval, $f_{T_A}(t)$ is the time to outage provided in (10), while $f_{T_A}(T_U)$ is given by

$$F_{T_A}(T_U) = Pr\{T_A < T_U\} = \int_0^{T_U} f_{T_A}(t)dt, \quad (57)$$

and represents the probability that the time to outage is smaller than the beamalignment interval.

For on-demand beamalignment, the intensity of UE state changes is thus $\nu_M = p_{O,1}/T_B$. For periodic beamalignment, however, the outage time does not necessarily coincide with the beamalignment time as the non-outage time T_A might be smaller than T_U. The mean outage time in this case is

$$T_{O,2} = \begin{cases} T_B/(T_U + T_B), & T_A \geq T_U, \\ (T_U + T_B - T_A)/(T_U + T_B), & T_A < T_U, \end{cases} \quad (58)$$

leading to the following intensity of UE state changes

$$\nu_M = \frac{\frac{T_B[1 - F_{T_A}(T_U)]}{T_U + T_B} + \int_0^{T_U} \frac{T_U + T_B - t}{T_U + T_B} f_{T_A}(t)dt}{\int_0^{T_U} (T_U + T_B - t)f_{T_A}(t)dt + [1 - F_{T_A}(T_U)]T_B}. \quad (59)$$

VI. Numerical Analysis

In this section, we numerically elaborate the association schemes and multi-connectivity strategies by utilizing the developed performance evaluation framework. We start our discussion with the effect of blockage on the new and ongoing session loss probabilities as well as mmWave BS resource utilization and then proceed with evaluating the impact of micromobility, and radio part parameters. The coverage radii of mmWave and THz BSs for the considered association schemes are presented in Table III, while the default parameters utilized in our numerical study are summarized in Table II. With respect to the propagation model, we utilize computer simulations to derive interference, SINR, and resource request distribution as discussed in Section V.

As shown in [5], the effect of Cartesian displacements, Δx and Δy, is negligible compared to yaw and pitch mobilities. Thus, in the rest of this section, we concentrate on the effect of the latter parameters and keep Δx and Δy constant at 3 cm/s. Also, below we demonstrate results for on-demand beamalignment scheme and applications characterized by outage sensitivity $T_O = T_B$, where T_B is the beamalignment time.

A. Effect of Blockage

1) Outage Avoidance Association, A1: We start our analysis with comparison of multi-connectivity strategies for A1 association scheme, where UEs are associated with THz BSs only when blockage does not lead to outage. To this aim, Fig. 4 illustrates new and ongoing session loss probabilities as well as system resource utilization for different multi-connectivity strategies, S1-S4, as a function of the blockers intensity, $C = 10$ Mbps, $\Delta\phi = \Delta\theta = 0.1$ °/s, 8×4 and 64×4 mmWave and THz BS antenna arrays, respectively, the number of THz BS in the coverage of mmWave BS $N = 5$, and session arrival intensity of 10^{-4} sessions/s/m^2. Recall, that for the considered association scheme blockage does not affect the service process of sessions that are initially associated with THz BSs. However, it does cause reallocation of resources for sessions at mmWave BS. Furthermore, sessions originally associated with THz BSs are affected by the micromobility. The latter two effects cause
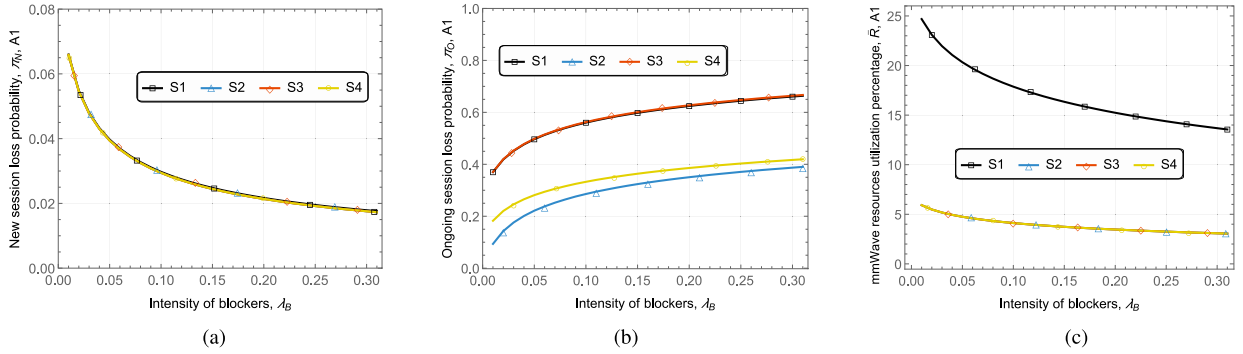
Fig. 4. Considered performance metrics for A1 association scheme and different multi-connectivity strategies. (a) New session loss probability. (b) Ongoing session loss probability. (c) System resource utilization.

TABLE II
THE DEFAULT SYSTEM PARAMETERS

Notation	Description	Values
$f_{M,c}, f_{T,c}$	mmWave/THz carrier frequency	28/300 GHz
B_M, B_T	mmWave/THz bandwidth	0.4/4 GHz
C	required session rate	10 Mbps
μ^{-1}	mean session service time	10 s
K	number of THz BSs	3-8
λ_A	session arrival intensity	10^{-4} ses./s/m^2
λ_B	density of blockers	0.1 bl./m^2
h_B, r_B	blocker height and radius	1.7/0.4 m
$h_{T,B}$	THz BS height	10 m
$h_{M,B}$	mmWave BS height	10 m
h_U	UE height	1.7 m
v_B	UE speed	1 m/s
P_M, P_T	mmWave/THz BS emitted power	2 W
$\zeta_{M,i}, \zeta_{T,i}, i = 0, 1$	path loss exponents in nLoS state	3.19
$\zeta_{M,i}, \zeta_{T,i}, i = 2, 3$	path loss exponents in LoS state	2.1
$N_{T,B,V}, N_{T,B,H}$	THz BS antenna configuration	16×4
$N_{T,U,V}, N_{T,U,H}$	THz BS antenna configuration	4×4
$N_{M,B,V}, N_{M,B,H}$	mmWave BS antenna configuration	8×4
$N_{M,U,V}, N_{M,U,H}$	mmWave UE antenna configuration	4×4
N_0	thermal noise power	-84 dBi
$\Delta x, \Delta y$	mean displacement over $0x$ and $0y$	0.03 m/s
$\sigma_{M,i}$	st. dev. of mmWave shadow fading	7/7/4/4 dB
$\sigma_{T,i}$	st. dev. of mmWave shadow fading	8/8/5/5 dB
$V_{M,i}$	THz Nakagami-m parameters	2/2/3/3
$V_{T,i}$	mmWave Nakagami-m parameters	3/3/4/4
$\Delta\phi, \Delta\theta$	mean yaw/pitch displacement	0.1°/s
β_B	recovery intensity for blockage	1.25 events/s
β_M	recovery intensity for micromob.	1800 events/s
T_B	beamalignment time	$1/\beta_M$ s
T_O	application outage tolerance time	$= T_B$ s
$p_{M,O}, p_{T,O}$	mmWave/THz cell edge outage	0.05
J	number of MCSs	15

the increase in the ongoing session loss probability for all the considered multi-connectivity strategies as evident from Fig. 4(b). However, the underlying reason is different for S1/S3 multi-connectivity strategies as compared to S2/S4. Recall, that for S1/S3 micromobility always leads to the loss of sessions. For this reason, the ongoing session loss probability coincides for these schemes. Further, S2 presumes the use of outage non-sensitive applications that can tolerate outage caused by antenna misalignment and thus the value on the considered parameter is lowest out of all the considered strategies. Notice that it is still not negligible as reallocation of the resources for sessions due

to blockage at mmWave BS leads to consistent increase in this metric as blockers' intensity increases. Finally, as S4 assumes that micromobility always causes rerouting from THz BS to mmWave BS it leads to "intermediate" values of the ongoing session loss probabilities as some of the sessions switched over to mmWave BS are lost due to insufficient available resources.

Observe that Fig. 4(a) shows that the new session loss probabilities coincide for all the considered multi-connectivity strategies. The rationale is that for A1 association scheme only micromobility may cause additional load at mmWave BS as sessions that may experience outage at THz BSs are accepted to mmWave BS. However, the time to align the antenna beams is very small producing negligible load at mmWave BS leading to the same performance for all the considered multi-connectivity strategies.

Analyzing the data presented in Fig. 4 further, one may observe that there is a trade-off between new and ongoing session loss probabilities for all the considered multi-connectivity strategies. Specifically, as the former metric decreases with blockers' intensity, the latter – increases. The reason is that the increase in the ongoing session loss probability leads to more resources available for new sessions. These conclusions are also supported by the mmWave BS resource utilization which decreases with the blockage intensity λ_B. Observe that for the same new and ongoing session loss probabilities smaller resource utilization of mmWave BS implies overall better offloading performance of the system as more sessions are served at THz BS. By analyzing the data presented in Fig. 4(c) one may conclude that S2/S4 strategies show better THz BSs resource utilization compared to S1/S3 strategies.

2) Coverage Enhancement Association, A2: Having studied the association scheme A1, where a session that may experience outage in case of blockage at THz BSs is routed to mmWave BS, we now proceed assessing A2 association scheme, where these sessions are accepted at THz BSs. To this aim, Fig. 5 shows new and ongoing session loss probabilities as well as system resource utilization for different multi-connectivity strategies and the same parameters as in Fig. 4. Here, one may observe that the qualitative behavior of the metrics is reversed. More specifically, the new session loss probability increases as opposed to the
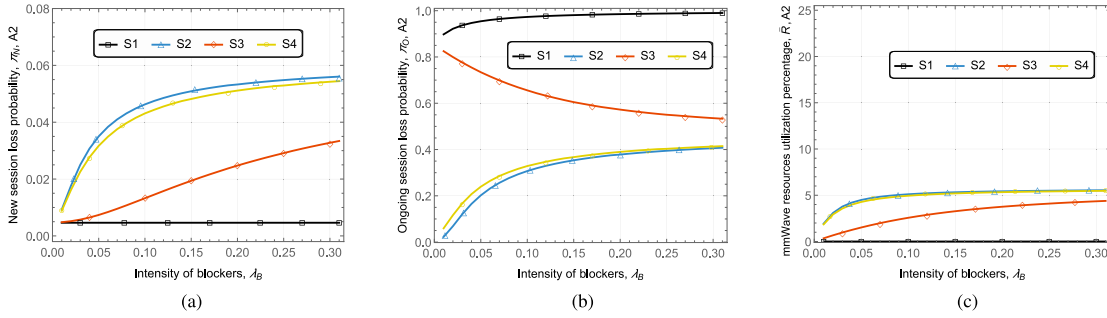
Fig. 5. Considered performance metrics for A2 association scheme and different multi-connectivity strategies. (a) New session loss probability. (b) Ongoing session loss probability. (c) System resource utilization.

decrease for A1. While the rationale for this behavior is generally attributed to blockage at THz BSs that leads to handing sessions over to the mmWave BS, there are specifics for each considered multi-connectivity strategy.

First of all, the simplest multi-connectivity strategy that showed relatively good performance for A1 association scheme, S1, where no rerouting is performed in case of outage at THz BS, now is characterized by the absolute worst performance. More specifically, for A2 association scheme, this strategy accepts almost all the sessions to the THz BSs but all of those are eventually lost due to blockage and micromobility. In contrast, the multi-connectivity strategy S4, where both micromobility and outage at THz BSs causes change of the association point to mmWave BS, is characterized by similar ongoing session loss probability to A1 association scheme but has an increased new session loss probability. However, notice that in the negligible blockers density regime, i.e., $\lambda_B < 0.1$ bl./m^2, S4 multi-connectivity strategy outperforms any other strategy for A1/A2 association schemes and can be generally recommended for network operators.

Logically, S2 multi-connectivity strategy, characterizing performance of applications non-sensitive to short-term outage caused by micromobility, is associated with slightly better ongoing session loss probability but worse new session loss probability. For A2 association scheme unique strategy is S3, where no actions is taken against micromobility resulting in session losses, but blockage is avoided by handing the session over to mmWave BS. For this strategy, the ongoing session loss probability decreases with blockers density but the associated increase in the new session loss probability is milder compared to S2 and S4 strategies. The rationale is that with the increase of the blockers density λ_B, the probability that the session is rerouted to mmWave BS increases diminishing the chances of session being dropped due to micromobility at THz BSs. In spite A2/S3 combo still loses to A1/S4, it might be a viable option for future THz/mmWave deployments.

Thus, we may conclude that accepting sessions to THz BSs that may experience outage in case of blockage is generally worse as compared to serving them at mmWave BS for non-negligible blockers density. Contrarily, for $\lambda_B < 0.1$ the combination of A1 association scheme and S2/S4 multi-connectivity strategies show the best performance.

3) The Ongoing Session Loss Probability: The considered multi-connectivity strategies, S2-S4, are characterized by two
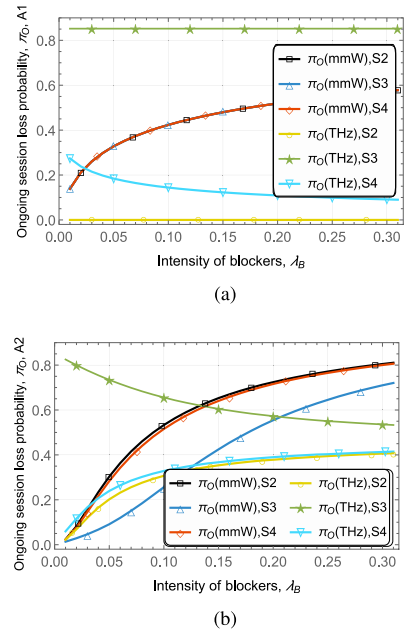

Fig. 6. Components contributing to the ongoing session loss probability. (a) Association scheme A1. (b) Association scheme A2.

components contributing to the ongoing session loss probability: (i) losses at mmWave BS as a result of LoS blockage and subsequent unsuccessful attempt of resource reallocation and, (ii) losses as a result of rerouting from THz BSs to mmWave BS. To understand the structure of the considered metric, Fig. 6 presents these components as a function of the blockers' density for the same system parameters as in Fig. 4, Fig. 5.

Analyzing the presented data, one may observe that for the association scheme A1, the ongoing session loss probability at the mmWave BS coincide for all the considered schemes and increase with the blockers' density. The main reason is reallocation of resources caused by sessions currently served at mmWave BS and switching from non-blocked to blocked states. The component associated with the session loss at THz BS is constant at zero for outage non-sensitive applications (S2 strategy) and is maximized for strategy S3, where no actions is taken in case of micromobility. Finally, the strategy S4 is characterized by the decreasing loss probability at THz BSs. Still, the increase caused by session loss at mmWave BS prevails leading to the associated increase in Fig. 4(b).
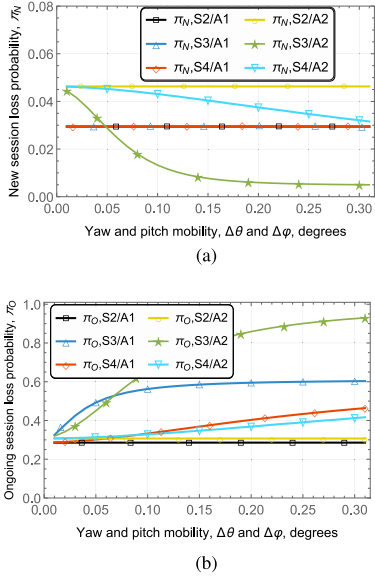
Fig. 7. The impact of micromobility on session loss probabilities. (a) New session loss probability. (b) Ongoing session loss probability.

Fig. 8. The impact of traffic load and antenna arrays (A1). (a) New session loss probability. (b) Ongoing session loss probability.

For A2 association scheme, where the session is accepted to THz BSs even when blockage leads to outage, mmWave BS loss components are all increasing functions of λ_B. However, the behavior of session loss probability associated with THz BS is different. The reason is the interplay between blockage and micromobility processes at THz BS. For S2 multi-connectivity strategy, where outage non-sensitive applications capable of surviving beamalignment caused by micromobility are assumed, the ongoing session loss probability at THz BS increases. The reason is session reroutes to mmWave BS caused by blockage. However, for S3 multi-connectivity strategy, where micromobility leads to the loss of sessions the increase in the blockers' density increases the ongoing session loss probability at THz BS. This component dominates leading to the trends observed in Fig. 5(b).

B. Effect of Micromobility

As we have already observed, the presence of micromobility provides significant impact of the system performance. To investigate the extent of this impact we now study the response of the new and ongoing session loss probabilities to the yaw and pitch mobilities, $\Delta\phi = \Delta\theta$, in Fig. 7 for $C = 10$ Mbps, blockers density of $\lambda_B = 0.1$ bl./m², 8×4 and 64×4 mmWave and THz BS antenna arrays, respectively, the number of THz BS in the coverage of mmWave BS $N = 5$, and session arrival intensity of 10^{-4} sessions/s/m².

By analyzing the data presented in Fig. 7, one may observe that all qualitative trends remain intact over the considered range of micromobility speeds. For A1 association scheme, where sessions are only accepted to THz BSs when blockage does not lead to outage, the new session loss probabilities remain unaffected by the micromobility speed. Specifically, micromobility does not affect S2 strategy at all, as the application is assumed to tolerate beamalignment time. For S3 and S4 strategies, micromobility speed does impact ongoing session loss probability and in the
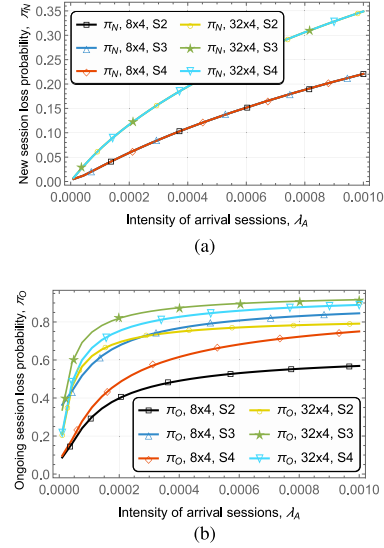
case of S4 also the load imposed at mmWave BS. However, the effect of the beamalignment time is negligible producing almost no impact on the mmWave BS load and thus the new session loss probability.

The situation is drastically different for A2 association scheme, where a session can be accepted to THz BS even when blockage may lead to outage conditions. Here, we see the significant decrease in the new session loss probabilities as a result of reduced load imposed on mmWave BS due to significantly higher ongoing session losses, see Fig. 7(b). Noticeably, the ongoing session loss probability is impacted most by strategy S3 for both A1 and A2 association schemes, where no actions are taken in case of micromobility events. The S4 strategy allows to effectively eliminate even extremely high micromobility speeds reaching 0.3 °/s, while the strategy S2 is logically not affected at all. Concluding, we may state that the micromobility speed does not qualitatively change the conclusions stated above for association schemes and multi-connectivity strategies.

C. Effects of the Traffic, Arrays, and Session Rate

We now evaluate whether session arrival intensity or radio part parameters affect the abovementioned conclusions. To this aim, Fig. 8 show the new and ongoing session loss probabilities as a function of the session arrival rate for A1 association scheme, two configurations of the mmWave BS antenna array, 8×4 and 32×4, $C = 10$ Mbps, $\lambda_B = 0.1$ bl./m², $\Delta\phi = \Delta\theta = 0.1$ °/s, 64×4 THz BS antenna array, and $N = 5$.

As one may observe, the behavior of the new and ongoing session loss probabilities is preserved across the whole range of the offered traffic load. Logically, for a given antenna configuration, the new session loss probabilities coincide for all the considered multi-connectivity strategies. However, there is clear difference between performance associated with the utilized antenna arrays at mmWave BS. More specifically, the system with 8×4 arrays is characterized by significantly lower new and ongoing session loss probabilities as compared to the one

TABLE III
SERVICE RADIUS OF THZ AND MMWAVE BS

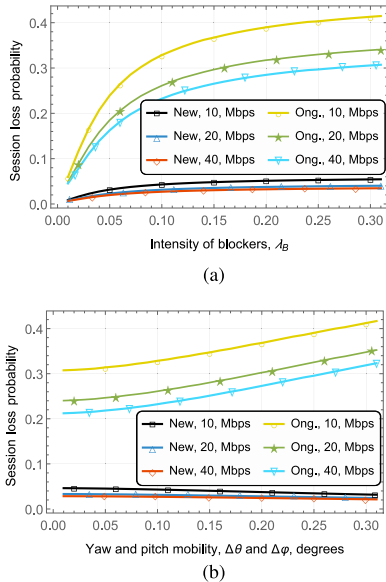| UE array	4x4	4x4	4x4
BS array	mmWave	THz A1	THz A2
8x4	73.3	-	-
16x4	91.3	-	-
32x4	113.6	-	-
64x4	-	20.1	92.1
128x4	-	25.7	114.4
256x4	-	32.6	142.2

Fig. 9. The impact of session rate on loss probabilities. (a) As a function of blockers intensity. (b) As a function of micromobility.

with 32×4 array. The rationale for this behavior is however attributed to the densification property as the system with 32×4 array covers much larger area (see Table III) and is thus faced with higher traffic arrival intensity.

Finally, we consider the effect of the session rate. To this aim, Fig. 9 shows the new and ongoing session loss probabilities for different session rates as a function of blockers density A2 association and S4 mutliconnectivity schemes, 8×4 and 64×4 mmWave and THz antenna arrays, and $N = 5$. As one may observe, the change in the session rates leads to quantitative and proportional change in the considered metrics.

VII. CONCLUSION

Motivated by the need to ensure service reliability of non-elastic rate-greedy applications in future 6G deployments featuring both mmWave and THz BS, we have analyzed the service process of such type of traffic in joint THz and mmWave cellular systems supporting multi-connectivity operation and subject to both blockage and micromobility impairments. To perform analysis of various user association schemes and multi-connectivity strategies, we have developed a unified mathematical framework simultaneously capturing radio and service specifics at the THz and mmWave BSs.

Our numerical analysis demonstrates that, when utilizing multi-connectivity at UEs, for high blockers density

environment, i.e., $\lambda_B > 0.1$ bl./m², only those sessions that does not experience outage in case of blockage, should be accepted for service at THz BSs. Otherwise, the coverage range of THz BSs can be enlarged by accepting also those sessions that may experience outage. Out of all the considered multi-connectivity strategies, the one that reroutes the session in case of both outage and multi-connectivity demonstrates consistently good results over the whole considered range of parameters. However, in this context, ensuring that the session may tolerate short-term outages caused by antenna misalignment at THz BSs is crucial as it greatly improves service reliability. Finally, under low blockage and micromobility conditions, the strategy that does not utilize multi-connectivity at all is characterized by the competitive performance. This is critical observation as it may simultaneously allow for energy conservation as supporting multi-connectivity is known to be energy consuming functionality [40].

Comparing the obtained results to those provided in [14] for "sub-6 GHz+mmWave" system we emphasize that "mmWave+THz" system is currently free of resource seizure effects, where the temporal offloading of mmWave sessions causes massive session losses at sub-6 GHz BSs. Thus, as opposed to the "mmWave+THz" systems considered in our study, the use of sub-6 GHz BSs to serve mmWave sessions is only feasible in light traffic conditions. However, we stress that this conclusion remains valid for the current session rates in the order of 10-100 Mbps (that includes yet to be deployed applications such as XR/VR applications, holographic communications) as mmWave band can be utilized to temporally support multiple tens of that simultaneously.

APPENDIX A
ACCOUNTING FOR FINITE CAPACITY AT THZ BSs

Here, we describe the changes needed in the performance evaluation framework to account for the limited capacity of THz BSs. In this case, THz BSs should be also modeled in the terms of resource queuing systems. So, let N_k, $k = 1, 2, \ldots, K$ be the maximum number of sessions that can be served simultaneously on kth BS, and R_k, $k = 1, 2, \ldots, K$ – the number of resource units. For the strategy S1 (no multi-connectivity), in which the service process on THz and mmWave BSs are independent of each other, the model of a THz BS will be similar to the model of mmWave BS with the only difference in the number of flows. Due to additional micromobility-driven outages in THz links, the model will have three arrival flows: i) initially arriving sessions, ii) secondary sessions that were rerouted to mmWave due to blockage, iii) secondary sessions that were rerouted due to micromobility. Similarly to section IV, several arrival flows may be aggregated in one flow with weighted average resource requirements distribution.

With the limited capacity, the THz BS will also suffer from the session loss upon arrivals, and the corresponding probabilities $\pi_{a,k}$, $k = 1, 2, \ldots, K$ will be calculated similarly to formula (20) for the mmWave BS.

For the strategies S2-S4, an additional effect appears, caused by the limited capacity on THz BS. An accepted and then rerouted session can be dropped not only on the arrival to mmWave BS, but also on the return back to THz BS. So, the
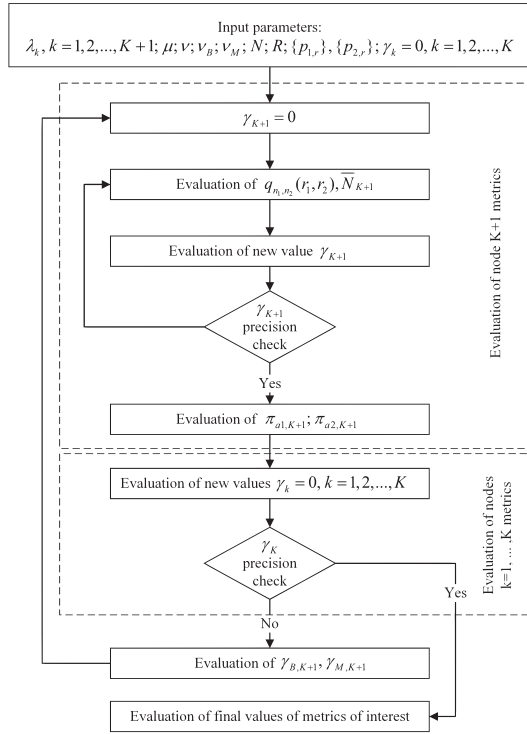
Fig. 10. Block diagram of the iterative algorithm.

serving process on THz BSs will be described by resource queuing systems with three arrival flows as for S1 strategy. Then, we introduce an additional probabilities $\pi_{b,k}$ and $\pi_{m,k}$, $k = 1, 2, \ldots, K$ that a rerouted THz session is dropped (b means rerouted due to blockage, and m – due to micromobility events)

$$\pi_{m,k} = \pi_{a2,K+1} + (1 - \pi_{a2,K+1})\frac{\beta_M}{\mu + \beta_M}\pi_{a,k},$$

$$\pi_{b,k} = \pi_{a2,K+1} + (1 - \pi_{a2,K+1})\frac{\beta_B}{\mu + \beta_B}\pi_{a,k}. \quad (60)$$

Finally, the probability $\pi_{s,k}$ that an accepted THz session is dropped during its service takes the following form:

$$\pi_{s,k} = \frac{\bar{N}_k(\nu_B\pi_{b,k} + \nu_M\pi_{m,k})}{\lambda_k(1 - \pi_{a,k})}. \quad (61)$$

The main idea of the iterative algorithm for calculating performance metrics of interest presented in Appendix B remains unchanged. However, the need for estimating stationary distributions of the resource queuing system at each iteration will significantly increase the computational complexity.

APPENDIX B
ALGORITHM FOR CALCULATING PERFORMANCE METRICS

Calculation of (24) requires an iterative algorithm shown in Fig. 10. The algorithm starts with the evaluation of metrics at node $K + 1$ with only primary session arrivals ($\gamma_{K+1} = \gamma_{B,K+1} = \gamma_{M,K+1} = 0$). Stationary distribution $q_{n_1,n_2}(r_1, r_2)$, see (17) and (18), and average number of primary and secondary sessions $\bar{N}_{1,K+1}$ in (19) are calculated. Using the obtained value

of $\bar{N}_{1,K+1}$, the new value of the secondary sessions arrival intensity γ_{K+1} is calculated according to (13). If the modulo of the difference between the new and the previous values of γ_{K+1} is greater than the predefined precision level, the algorithm proceeds to the new iteration. If the desired precision is achieved, the session loss probabilities $\pi_{a1,K+1}$ and $\pi_{a2,K+1}$ are obtained according to (20). Besides, the new values of γ_k are evaluated using (24). Again, if the modulo of the difference between the new and the previous values of γ_k is greater than the precision level, the arrival intensities $\gamma_{B,K+1}$, $\gamma_{M,K+1}$ of the rerouted sessions at node $K + 1$ are calculated according to (14), and the algorithm returns to the evaluation of stationary probabilities with new arrival intensities of rerouted sessions and no secondary sessions, i.e. $\gamma_{K+1} = 0$. Otherwise, the stable solution is achieved, and the algorithm proceeds to calculation of final metrics.

REFERENCES

[1] M. Shafi, H. Tataria, A. F. Molisch, F. Tufvesson, and G. Tunnicliffe, "Real-time deployment aspects of C-band and millimeter-wave 5G-NR systems," in *Proc. IEEE Int. Conf. Commun.*, 2020, pp. 1–7.

[2] M. Giordani, M. Polese, M. Mezzavilla, S. Rangan, and M. Zorzi, "Toward 6G networks: Use cases and technologies," *IEEE Commun. Mag.*, vol. 58, no. 3, pp. 55–61, Mar. 2020.

[3] B. A. Bilgin, H. Ramezani, and O. B. Akan, "Human blockage model for indoor terahertz band communication," in *Proc. IEEE Int. Conf. Commun. Workshops*, 2019, pp. 1–6.

[4] J. M. Jornet and I. F. Akyildiz, "Channel modeling and capacity analysis for electromagnetic wireless nanonetworks in the terahertz band," *IEEE Trans. Wireless Commun.*, vol. 10, no. 10, pp. 3211–3221, Oct. 2011.

[5] V. Petrov, D. Moltchanov, Y. Koucheryavy, and J. M. Jornet, "Capacity and outage of terahertz communications with user micro-mobility and beam misalignment," *IEEE Trans. Veh. Technol.*, vol. 69, no. 6, pp. 6822–6827, Jun. 2020.

[6] N. Stepanov, D. Moltchanov, A. Turlikov, and Y. Koucheryavy, "Statistical analysis and modeling of user micromobility for THz cellular communications," *IEEE Trans. Veh. Technol.*, vol. 71, no. 1, pp. 725–738, Jan. 2022.

[7] R. Vannithamby and S. Talwar, *Towards 5G: Applications, Requirements and Candidate Technologies*. Hoboken, NJ, USA: Wiley, 2017.

[8] 3GPP, "NR; Multi-connectivity; stage 2," 3GPP TS 37.340 V17.0.0, 3GPP, Apr. 2022.

[9] M. Polese, M. Giordani, M. Mezzavilla, S. Rangan, and M. Zorzi, "Improved handover through dual connectivity in 5G mmWave mobile networks," *IEEE J. Sel. Areas Commun.*, vol. 35, no. 9, pp. 2069–2084, Sep. 2017.

[10] F. B. Tesema, A. Awada, I. Viering, M. Simsek, and G. P. Fettweis, "Mobility modeling and performance evaluation of multi-connectivity in 5G intra-frequency networks," in *Proc. IEEE Globecom Workshops*, 2015, pp. 1–6.

[11] M. Gapeyenko et al., "On the degree of multi-connectivity in 5G millimeter-wave cellular urban deployments," *IEEE Trans. Veh. Technol.*, vol. 68, no. 2, pp. 1973–1978, Feb. 2019.

[12] V. Begishev et al., "Joint use of guard capacity and multiconnectivity for improved session continuity in millimeter-wave 5G NR systems," *IEEE Trans. Veh. Technol.*, vol. 70, no. 3, pp. 2657–2672, Mar. 2021.

[13] D. Moltchanov et al., "Performance characterization and traffic protection in street multi-band millimeter-wave and microwave deployments," *IEEE Trans. Wireless Commun.*, vol. 21, no. 1, pp. 163–178, Jan. 2022.

[14] V. Begishev et al., "Performance analysis of multi-band microwave and millimeter-wave operation in 5G NR systems," *IEEE Trans. Wireless Commun.*, vol. 20, no. 6, pp. 3475–3490, Jun. 2021.

[15] V. Petrov, M. Komarov, D. Moltchanov, J. M. Jornet, and Y. Koucheryavy, "Interference and SINR in millimeter wave and terahertz communication systems with blocking and directional antennas," *IEEE Trans. Wireless Commun.*, vol. 16, no. 3, pp. 1791–1808, Mar. 2017.

[16] J. Kokkoniemi, J. Lehtomäki, and M. Juntti, "Stochastic geometry analysis for mean interference power and outage probability in THz networks," *IEEE Trans. Wireless Commun.*, vol. 16, no. 5, pp. 3017–3028, May 2017.

[17] A. Shafie, N. Yang, S. Durrani, X. Zhou, C. Han, and M. Juntti, "Coverage analysis for 3D terahertz communication systems," *IEEE J. Sel. Areas Commun.*, vol. 39, no. 6, pp. 1817–1832, Jun. 2021.

[18] Y. Wu, J. Kokkoniemi, C. Han, and M. Juntti, "Interference and coverage analysis for terahertz networks with indoor blockage effects and line-of-sight access point association," *IEEE Trans. Wireless Commun.*, vol. 20, no. 3, pp. 1472–1486, Mar. 2021.

[19] A. Shafie, N. Yang, and C. Han, "Multi-connectivity for indoor terahertz communication with self and dynamic blockage," in *Proc. IEEE Int. Conf. Commun.*, 2020, pp. 1–7.

[20] D. Moltchanov, Y. Gaidamaka, D. Ostrikova, V. Beschastnyi, Y. Koucheryavy, and K. Samouylov, "Ergodic outage and capacity of terahertz systems under micromobility and blockage impairments," *IEEE Trans. Wireless Commun.*, vol. 21, no. 5, pp. 3024–3039, May 2022.

[21] W. Wang, J. Wu, N. Li, and R. Song, "Joint User Association and Resource Allocation for Mmwave and THz Coexistence Networks," in *Proc. IEEE Int. Conf. Parallel Distrib. Process. Appl. Big Data Cloud Comput. Sustain. Comput. Commun. Social Comput. Netw.*, 2021, pp. 1287–1294.

[22] N. Hassan, M. T. Hossan, and H. Tabassum, "User association in coexisting RF and terahertz networks in 6G," in *Proc. IEEE Can. Conf. Elect. Comput. Eng.*, 2020, pp. 1–5.

[23] 3GPP, "NR; Physical Channels and Modulation," TS 38.211, V 17.2.0, 3GPP, Jun. 2022.

[24] V. Petrov, T. Kurner, and I. Hosako, "IEEE 802.15. 3D: First standardization efforts for sub-terahertz band communications toward 6G," *IEEE Commun. Mag.*, vol. 58, no. 11, pp. 28–33, Nov. 2020.

[25] P. Nain, D. Towsley, B. Liu, and Z. Liu, "Properties of random direction models," in *Proc. IEEE 24th Annu. Joint Conf. IEEE Comput. Commun. Soc.*, 2005, vol. 3, pp. 1897–1907.

[26] M. Gapeyenko et al., "Analysis of human-body blockage in urban millimeter-wave cellular communications," in *Proc. IEEE Int. Conf. Commun.*, 2016, pp. 1–7.

[27] 3GPP, "Study on Channel Model for Frequencies From 0.5 to 1226 100 GHz," 3GPP TR 38.901, V 17.0.0, 3GPP, Mar. 2022.

[28] S. Singh, R. Mudumbai, and U. Madhow, "Interference analysis for highly directional 60-GHz mesh networks: The case for rethinking medium access control," *IEEE/ACM Trans. Netw.*, vol. 19, no. 5, pp. 1513–1527, Oct. 2011.

[29] C. A. Balanis, *Antenna Theory: Analysis and Design*. New York, NY, USA: John wiley & sons, 2015.

[30] G. R. MacCartney, S. Deng, S. Sun, and T. S. Rappaport, "Millimeter-wave human blockage at 73 GHz with a simple double knife-edge diffraction model and extension for directional antennas," in *Proc. IEEE 84th Veh. Technol. Conf.*, 2016, pp. 1–6.

[31] L. S. Rothman et al., "HITRAN: High-resolution transmission molecular absorption database," *Tech. Rep*, Harvard-Smithson Center for Astrophysics, 2014. [Online]. Available: www.cfa.harvard.edu

[32] R. Kovalchukov, D. Moltchanov, A. Samuylov, S. Andreev, Y. Koucheryavy, and K. Samouylov, "Evaluating SIR in 3D millimeter-wave deployments: Direct modeling and feasible approximations," *IEEE Trans. Wireless Commun.*, vol. 18, no. 2, pp. 879–896, Feb. 2019.

[33] V. Naumov, Y. Gaidamaka, N. Yarkina, and K. Samouylov, *Matrix and Analytical Methods for Performance Analysis of Telecommunication Systems*. Berlin, Germany: Springer, 2021.

[34] V. A. Naumov, K. E. Samuilov, and A. K. Samuilov, "On the total amount of resources occupied by serviced customers," *Automat. Remote Control*, vol. 77, no. 8, pp. 1419–1427, 2016.

[35] E. S. Sopin, K. A. Ageev, E. V. Markova, O. G. Vikhrova, and Y. V. Gaidamaka, "Performance analysis of M2M traffic in LTE network using queuing systems with random resource requirements," *Autom. Control Comput. Sci.*, vol. 52, no. 5, pp. 345–353, 2018.

[36] T. Bai and R. W. Heath, "Coverage and rate analysis for millimeter-wave cellular networks," *IEEE Trans. Wireless Commun.*, vol. 14, no. 2, pp. 1100–1114, Feb. 2015.

[37] S. Ross, *Introduction to Probability Models*. Cambridge, MA, USA: Academic Press, 2010.

[38] M. Gapeyenko et al., "On the temporal effects of mobile blockers in urban millimeter-wave cellular scenarios," *IEEE Trans. Veh. Technol.*, vol. 66, no. 11, pp. 10124–10138, Nov. 2017.

[39] J. W. Cohen, *The Single Server Queue*. Amsterdam, Netherlands: Elsevier, 2012.

[40] Y.-N. R. Li, M. Chen, J. Xu, L. Tian, and K. Huang, "Power saving techniques for 5G and beyond," *IEEE Access*, vol. 8, pp. 108675–108690, 2020.

Eduard Sopin received the B.Sc. and M.Sc. degrees in applied mathematics from the Peoples' Friendship University of Russia, Moscow, Russia, in 2008 and 2010, respectively, and the Ph.D. degree in applied mathematics and computer science, in 2013. His current research interests include the performance analysis of modern wireless networks and cloud/fog computing.

Dmitri Moltchanov received the M.Sc. and Cand.Sc. degrees from the St. Petersburg State University of Telecommunications, Saint Petersburg, Russia, in 2000 and 2003, respectively, and the Ph.D. degree from the Tampere University of Technology, Tampere, Finland, in 2006. He is currently the University Lecturer with the Laboratory of Electronics and Communications Engineering, Tampere University. He has (co-)authored more than 150 publications on wireless communications, heterogeneous networking, IoT applications, applied queuing theory. His current research interests include research and development of 5G/5G+ systems, ultra-reliable low-latency service, industrial IoT applications, mission-critical V2V/V2X systems and blockchain technologies. During his career he has taught more than 50 full courses on wireless and wired networking technologies, P2P/IoT systems, network modeling, queuing theory, etc.

Anastasia Daraseliya received the B.Sc. and M.Sc. degrees in applied mathematics from the Peoples' Friendship University of Russia, Moscow, Russia, in 2016 and 2018, respectively. Her current research interests include the performance analysis of modern wireless networks and cloud/fog computing.

Yevgeni Koucheryavy received the Ph.D. degree from the Tampere University of Technology (TUT), Tampere, Finland. He is currently a Professor with the laboratory of electronics and communications engineering, TUT. He is the author of numerous publications in the field of advanced wired and wireless networking and communications. His current research interests include various aspects in heterogeneous wireless communication networks and systems, the Internet of Things and its standardization, and nanocommunications. He is the Associate Technical Editor of the IEEE Communications Magazine and an Editor of the IEEE COMMUNICATIONS SURVEYS AND TUTORIALS.

Yuliya Gaidamaka received the Ph.D. and Full Doctor of Sciences degrees in mathematics from the Peoples' Friendship University of Russia, Moscow, Russia, in 2001 and 2017, respectively. She is the author of more than 200 scientific and conference papers, co-author of three monographs on multiplicative solutions of finite Markov chains, matrix and analytical methods for performance analysis of wireless heterogeneous networks. Her current research interests include performance analysis of 5G+ networks, queuing theory, mathematical modeling of communication networks including admission control, and radio resource management using artificial intelligence.